

Review

A Review of Modelling of the FCC Unit—Part II: The Regenerator

Thabang W. Selalame, Raj Patel, Iqbal M. Mujtaba  and Yakubu M. John * 

Department of Chemical Engineering, Faculty of Engineering and Informatics, University of Bradford, Bradford BD7 1DP, UK; t.selalame@bradford.ac.uk (T.W.S.); r.patel@bradford.ac.uk (R.P.); I.M.Mujtaba@bradford.ac.uk (I.M.M.)

* Correspondence: Y.John@bradford.ac.uk

Abstract: Heavy petroleum industries, including the Fluid Catalytic Cracking (FCC) unit, are among some of the biggest contributors to global greenhouse gas (GHG) emissions. The FCC unit's regenerator is where these emissions originate mostly, meaning the operation of FCC regenerators has come under scrutiny in recent years due to the global mitigation efforts against climate change, affecting both current operations and the future of the FCC unit. As a result, it is more important than ever to develop models that are accurate and reliable at predicting emissions of various greenhouse gases to keep up with new reporting guidelines that will help optimise the unit for increased coke conversion and lower operating costs. Part 1 of this paper was dedicated to reviewing the riser section of the FCC unit. Part 2 reviews traditional modelling methodologies used in modelling and simulating the FCC regenerator. Hydrodynamics and kinetics of the regenerator are discussed in terms of experimental data and modelling. Modelling of constitutive parts that are important to the FCC unit, such as gas–solid cyclones and catalyst transport lines, are also considered. This review then identifies areas where the current generation of models of the regenerator can be improved for the future. Parts 1 and 2 are such that a comprehensive review of the literature on modelling the FCC unit is presented, showing the guidance and framework followed in building models for the unit.

Keywords: fluid catalytic cracking; regenerator; hydrodynamics; kinetics; modelling; coke combustion



Citation: Selalame, T.W.; Patel, R.; Mujtaba, I.M.; John, Y.M. A Review of Modelling of the FCC Unit—Part II: The Regenerator. *Energies* **2022**, *15*, 388. <https://doi.org/10.3390/en15010388>

Academic Editor: Dmitri A. Bulushev

Received: 21 October 2021

Accepted: 28 December 2021

Published: 5 January 2022

Publisher's Note: MDPI stays neutral with regard to jurisdictional claims in published maps and institutional affiliations.



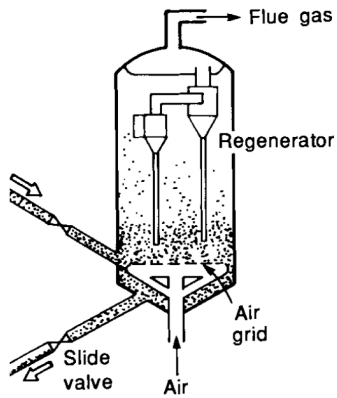
Copyright: © 2022 by the authors. Licensee MDPI, Basel, Switzerland. This article is an open access article distributed under the terms and conditions of the Creative Commons Attribution (CC BY) license (<https://creativecommons.org/licenses/by/4.0/>).

1. Introduction

Process modelling and simulation have been widely used in a vast number of industries to analyse, control and optimise the behaviour of different processes. The fundamental requirement for a model is that it be efficient and accurate at making the predictions that the end user is interested in. The deactivated catalyst is sent to the regenerator, where the coke on the catalyst is burned off. It has two main functions: (i) to burn off the coke on the catalyst to regain the catalyst's activity; (ii) to provide the heat needed to drive the endothermic cracking reactions in the riser-reactor via the exothermic combustion reactions [1]. The FCC regenerator is a complex fluidised bed reactor that is used for air combustions of catalytic coke deposited on catalyst during catalytic cracking of gas oil feedstock. The regenerator operates in the bubbling/turbulent regime of fluidisation, which results in complex hydrodynamics in terms of mass, momentum and energy transport phenomena, making it a difficult process to model [2,3]. The FCC regeneration process also results in the production of GHG emissions, mainly carbon dioxide, which makes it a significant contributor to climate change [4]. The recent global effort, through the Paris Agreement [5] and global treaties on the combat of climate change [6,7], mean it is more important than ever to build models of units such as the FCC regenerator that can accurately predict the emissions of GHGs. Such models allow for the optimisation of the unit so that emissions of various GHGs are minimised.

In Part 1 of this paper, we reviewed the literature on the modelling of the FCC riser; the current paper will present a similar analysis for the regenerator. The normal operating conditions of the regenerator are shown in Table 1.

Table 1. Dimensions and Operating conditions of FCC unit [8–12].

Regenerator	Dimensions	
	Height	30–40 m
	Diameter	1–2 m
	Operating Conditions	
	Gas oil inlet T	150–300 °C
	Catalyst inlet T	675–750 °C
	Catalyst exit T	500–550 °C
	Coke entering	0.5–1.5 wt%
	Coke leaving	0.15–0.35 wt%
	Pressure	200–400 KPa
	Solid Residence	$\sim \leq 1$ h

The literature on modelling the regenerator is vast and extensive. Because of the sheer complexity of the unit, many papers published on the topic have taken different approaches and to varying degrees of detail. Since much of the complexity in the system is a result of the hydrodynamics, models of the unit have usually benefitted from advancements in the modelling of cold flow bubbling and turbulent beds. Early work in this field was aimed at understanding such beds, such as developments of two-phase theory by Toomey and Johnstone [13]. This was followed by extensions to include the cloud and wake phase and incorporation of downflow of solids at the wall of the bed through back-mixing models [14–17]. These models were extensively used by various workers to model the regenerator hydrodynamics [1,10,18–20]. The reaction kinetics of the chemical reactions taking place in the regenerator has also been well studied and documented. Early work in this field dates back to Arthur [21], who studied the rates of combustion of uninhibited carbon in the form of graphite in air, establishing the existence of a temperature-dependent ratio of carbon monoxide (CO) to carbon dioxide (CO₂) produced when carbon burns in the air. Subsequent work studied the rates of combustion of catalytic coke deposited in porous alumina–silica particles, which were used as FCC catalysts in the 1960s [22–25]. Post-1970, there was a change in FCC catalyst that saw the replacement of alumina–silica catalyst by zeolitic catalysts. Subsequently, more kinetic studies using spent zeolite were published measuring the rates of the combustion reactions in these then-new catalysts [26–28]. Both sets of studies reported that the presence of some metals in the catalyst tended to affect the rates of oxidation reported catalytically. Workers have routinely coupled the hydrodynamics and the kinetics to produce regenerator models that can predict the conversion of coke and emissions of gases from the system. Post-2000, driven by the increase in computational power available to researchers and the need to understand the flow patterns involved in the gas–solid flow of the regenerator, saw the explosion in the number of papers using computational fluid dynamics (CFD) to simulate the regenerator [29–31]. These CFD models seem to represent the highest conceivable amount of rigor that is possible for any FCC regenerator model [18]. However, this current review is not concerned with CFD models, but only the classical models that average flow over the reactor cross section to produce one-dimensional (1D) or two-dimensional models (2D) is discussed here.

In Part 1 of this paper, we showed that there are already a few reviews of the FCC modelling literature; however, a comprehensive review of traditional FCC unit modelling approaches was found to be lacking in the literature. Of note was the lack of reviews that link experimental findings of operations of FCC unit to the traditional modelling

approaches and the simulation results obtained from said models. The current study presents a review of the modelling of the regenerator and analysing the experimental data that has led to the assumptions made in modelling. The modelling was divided in terms of kinetics, where treatments of reaction rate equations, rate constants and orders of reactions are considered, and in terms of hydrodynamics, where gas–solid mixing behaviour, flow, heat and mass transfer in the reactor are considered. Phase description is explained in the regenerator, and the issue of bubbles in the bed is also explained. In the end, the deficiencies of current regenerator models are identified, and recommendations for further work are made.

2. FCC Regenerator

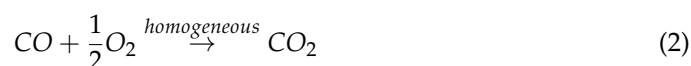
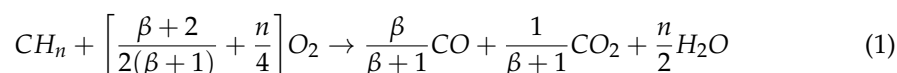
2.1. Regenerator Kinetics

A review of the literature on the combustion of coke on the catalyst in a regenerator reactor finds that there are generally four levels of complexity or considerations, i.e., (i) definition/composition of coke, (ii) rates and orders of reactions, (iii) the issue of conversion of CO to CO₂ and (iv) action from transition metals. All of these are discussed below. The main aim of the regenerator is to burn off the coke-on-catalyst in order to regain the activity of the spent catalyst. Additionally, the heat produced from these combustion reactions is used to power the endothermic cracking reactions in the riser. Kinetic studies in the regenerator are much simpler compared to that of the riser because, except for coke, the reacting species are generally known, and therefore, it is easier to generate the stoichiometric equations for the reactions taking place. This greatly simplifies the analysis in kinetic studies. During normal operation of the regenerator, two main combustion reactions occur: the combustion of coke and combustion of carbon monoxide that is produced via incomplete combustion of coke [25,27,28].

It has been long known that coke formed during catalytic cracking reactions in an FCC riser-reactor is a complex mixture of various chemical compounds, including hydrocarbons, sulphuric and nitrogenous compounds [10,32]. The exact nature and composition of coke have historically been difficult to ascertain, mainly because [33] (i) coke components are largely involatile and complex in nature, (ii) components are strongly adsorbed to the surface of the catalyst, and difficult to separate by conventional methods and (iii) coke concentration on the catalyst is very low (< 1%), which leads to sensitivity issues during characterisations. Nevertheless, several experimental techniques, such as elemental analysis, temperature-programmed oxidation (TPO), Fourier transform infrared spectroscopy (FT/IR), X-ray photoelectron spectroscopy (XPS), Thermogravimetric analysis, carbon-13 nuclear magnetic resonance (¹³C NMR), supercritical fluid extraction (SFE) and mass spectrometry and Raman spectroscopy, have been used by researchers to understand the nature and composition of coke better. Qian et al. [33] found chemical shift data in ¹³C NMR that distinguished between two types of carbon atoms in coke, namely aromatic (which makes up 70–90% of the coke) and aliphatic carbons. They also found, after deconvolution of the C_{1s} profiles in their XPS analysis, that carbon in the coke is primarily bonded to hydrogen, and that the existence of nitrogen is in both polar and non-polar functional groups. Nitrogen is typically present in the form of substituted polyaromatic compounds such as pyrroles (= C–NH₂), pyridines (–C–NC =) or anilines (= C–NH₂). Elemental analysis of Luan et al. [34] found that sulphur, present in the form of thiophene and thiols, is also a major component of coke. All these studies confirmed the complexity of coke in terms of structure and composition. However, for the purposes of modelling, in order to predict the evolution of gases released from coke combustion in the regenerator, the exact nature of the components of coke is not required as such an undertaking would be greatly tedious but to very little utility. Generally, only the elemental composition of coke is required. The relative elemental composition of coke is known to depend on the type of gas oil feed used for cracking and the cracking catalyst; therefore, these compositions are expected to vary depending on the specific operating parameters at a refinery [35]. It is also common practice that nitrogen and sulphur are considered negligible since their

molar composition is small compared to both hydrogen and carbon [1,32,36,37]. However, recent results from FT/IR elemental analysis by Luan et al. [34] may question the validity of this assumption as they have found spent catalyst to have a composition of 0.82 wt% carbon, 0.32% nitrogen, 0.71 wt% hydrogen and 0.76% sulphur, from analysis of flue gas emissions of the regenerator. These emission results show that both sulphur and nitrogen may be significant for some feeds and need to be included in the model description of coke. Another common assumption is the neglect of hydrogen so that coke is simplified to be equivalent to carbon. Bai et al. [37] argued that the hydrogen reaction's contribution to combustion in the regenerator should not be ignored as the burning rate of hydrogen can be up to two times that of carbon, and since the temperature is an important part of the FCC unit, it is, therefore, necessary to include hydrogen in the coke. Hence, most models of FCC units will model coke as CH_n , where n is the molar ratio of hydrogen to carbon in the coke. TPO studies of commercial spent equilibrium FCC catalysts by Bayraktar and Kugler [38] showed that n ranges from 0.45 to 0.96 (depending on the catalyst used and method of spent catalyst pre-treatment) for cracking of sour gas oil. This range is consistent with the range of 0.4–2.0 given by Hashimoto et al. [39].

The coke combustion inside an FCC regenerator can typically be described using a simple reaction scheme consisting of the following reactions in Equations (1)–(3):



where n is the molar ratio of hydrogen to carbon in the coke and β is the molar ratio of CO to CO₂. The subsequent oxidation of carbon monoxide is assumed to occur both on the surface of the catalyst (heterogeneous) and in the gaseous phase (homogeneous), with the reactions having different rates and hence the separate chemical reaction equations. Some studies noted the independent oxidation of carbon and hydrogen in the coke, allowing for the coke combustion equation to be split into two with separate equations for the oxidation of hydrogen and carbon [25]. Furthermore, several workers only consider carbon in coke and assume that the hydrogen is negligible [22,27,40]. Rate equations for the reactions are developed using the simple power law, where the rate of the reaction is a product of the kinetic parameter (given by the Arrhenius equation) and the concentrations (or partial pressures) of the reacting species raised to some order, n . The purpose of the kinetic studies is to determine kinetic parameter, which includes the frequency factor and activation energy of the reaction and the orders of the reactions, which are all determined empirically from fitting reaction model to experimental data. However, it was noticed early on by Weisz and Goodwin that kinetic studies on the combustion of coke in porous catalyst particles encountered some mass transfer effects that affected the apparent rates of reaction. Weisz and Goodwin, in a series of publications [22–24], presented some significant work in the combustion of coke in porous silica-alumina catalysts. Their work essentially defines two modes, determined by temperature and the size of the porous particle, that control the rate of combustion of the coke: (1) intrinsic chemical kinetics-controlled region and (2) diffusion or mass transfer limited region. They report that for any sized particle, there exists a temperature beyond which the rate of combustion is limited by how quickly oxygen can diffuse to the reaction site. This is the type 2 combustion region. Below that temperature, the reaction can be assumed to be in region 1. In this mode, the 'true' temperature-dependent rate of reaction can be determined in the abundance of reactants. In order to achieve higher conversions of coke in the regenerator, it is desirable that operating conditions are such that no mass transfer limitations are present, which is the fundamental assumption made by most researchers modelling the regenerator.

Some of the early work on the combustion of carbonaceous deposits in the air was made by Arthur [21]. This paper by Arthur presented yet another important factor in the kinetic studies of combustion of the carbonaceous particle using analysis of evolved gas, which is the difference between the global CO/CO_2 ratio and the local ratio. The former measures the ratio of the gases at the outlet, while the latter is concerned with the ratio at the surface of the particle. At the surface of the combusting material, CO and CO_2 are produced via the reaction in Equation (1) at a certain β ratio, and subsequently, β decreases due to the effect of reactions in Equations (1) and (2). Arthur [21] carried out combustion experiments on two uninhibited carbon sources (artificial graphite and coal char) and used Phosphoryl Chloride ($POCl$) to inhibit any further oxidation of carbon monoxide in order to capture the local β ratio. They found that rate combustion was independent of the mass of carbon present but proportional to the partial pressure of oxygen raised to a power less than unity. They also concluded that the β ratio at the surface of combustion seems to be uniquely determined only by temperature, provided the combustion has no mass transfer limitations. The β they determined in their work is shown in Table 2. Although their work was performed on uninhibited carbon, which is far from the combustion of coke trapped in porous cracking catalyst, their results were nevertheless important to understanding the intrinsic rates of oxidation of carbon in the air.

In the intrinsic chemical kinetics mode, Weisz and Goodwin [23] found that the combustion of coke (i.e., carbon) in the porous alumina–silica catalyst was first order in carbon. They found that there is only a single reproducible rate constant for this reaction for any given temperature that was independent of the catalyst or source of the coke used and that this relation followed Arrhenius type relationship with temperature. They also reported that the coke combustion on Si–Al catalyst was similar to that of burning behaviour of uninhibited graphite previously reported by Arthur [21], which they believed suggested the existence of a basic, un-catalysed rate of combustion of carbonaceous deposit in porous solids. Tone et al. [25] looked at the combustion of carbon and hydrogen in coke separately and confirmed the first-order kinetics with respect to both, and to oxygen partial pressure, for the combustion of coke on Si–Al catalyst. With the switch to zeolitic catalysts in the FCC unit in the 1970s, some new combustions kinetics studies were carried out on these then-new catalysts. These workers [27,28,41] confirmed the first-order kinetics of combustions in terms of both carbon and hydrogen for coke on zeolite catalyst. The order of reaction with respect to oxygen partial pressure (or concentration) is generally reported as being first-order [25,26,28,41]. However, contrary to this, Arthur [21] reported that the rate of combustion of graphite showed proportionality with oxygen partial pressure but raised to a power less than unity. Although, as noted before, the worker in that study used $POCl$ to inhibit the subsequent oxidation of carbon monoxide due to incomplete combustion and conceded that the $POCl$ also has some inhibition effects on the carbon combustion reaction, hence this may account for the discrepancy in the reaction order for oxygen.

Table 2. Kinetic studies of FCC regenerator reactions.

Authors	$C + O_2 \rightarrow CO + CO_2$	$H + O_2 \rightarrow H_2O$	$CO + O_2 \xrightarrow{homo} CO_2$	$CO + O_2 \xrightarrow{het} CO_2$	Conditions and Fuels Burned	Model/Correlation
[21]	✓				Artificial graphite, coal char granules 460–900 °C	$\frac{CO}{CO_2} = 10^{3.4} \times \exp\left(-\frac{51,900}{RT}\right)$ $-r_4 = k_4 P_{CO}, -r_3 = k_3 n_C P_{O_2}$ $-r_2 = k_2 n_C P_{O_2}, -r_1 = k_1 n_C P_{O_2}$ $k_1 = 1.63 \times 10^6 \exp\left(-\frac{152,900}{RT}\right) (\text{kPa}^{-1} \text{s}^{-1})$
[25]	✓	✓		✓	Coked silica–alumina catalyst 467–560 °C	$k_2 = 424 \exp\left(-\frac{107,000}{RT}\right) (\text{kPa}^{-1} \text{s}^{-1})$ $k_3 = 10.8 \exp\left(-\frac{76,190}{RT}\right) (\text{kPa}^{-1} \text{s}^{-1})$ $k_4 = 6.58 \times 10^{-7} \exp\left(-\frac{57,600}{RT}\right) (\text{kmol kPa}^{-1} \text{s}^{-1} \text{g}_{\text{cat}}^{-1})$
[42]			✓		N/A	$-\frac{d[CO]}{dt} = k [CO][O_2]^{0.5} [H_2O]^{0.5}$ $k = 1.3 \times 10^{11} \exp\left(-\frac{125,000}{RT}\right) (\text{m}^3 \text{kmol}^{-1} \text{s}^{-1})$
[26]	✓				Coked Zeolite CDY, Alkaline ex-change zeolites (MgY, AlY), Transition metal exchanged zeolite (CrY, CoY, CuY) 400–500 °C	$-\frac{dC}{dt} = k P_{O_2} C$ $k = 2.96 \exp\left(-\frac{109,600}{RT}\right) (\text{m}^3 \text{kPa}^{-1} \text{s}^{-1})$
[27]	✓				Coked Zeolites CRC-1, Y-7, Y-9 600–800 °C	$\frac{d(CO+CO_2)}{dt} = k C P_{O_2}$ $k = 2.75 \times 10^3 \exp\left(-\frac{161,000}{RT}\right) (\text{m}^3 \text{kPa}^{-1} \text{s}^{-1})$
[41]	✓	✓			Coked Zeolite catalyst 650–700 °C	$-r_C = \frac{k_C C_C CO_2}{M r_C}$ $k_C = 1.4 \times 10^8 \exp\left(-\frac{125,000}{RT}\right) (\text{m}^3 \text{kmol}^{-1})$

Table 2. Cont.

Authors	$C + O_2 \rightarrow CO + CO_2$	$H + O_2 \rightarrow H_2O$	$CO + O_2 \xrightarrow{homo} CO_2$	$CO + O_2 \xrightarrow{het} CO_2$	Conditions and Fuels Burned	Model/Correlation
[28]	✓	✓	✓		Coked OCTYDINE 1169 BR catalyst 620–720 °C	$-r_C = k_C C_C P_{O_2}$ $-r_{CO} = 2k_{CO} P_{O_2} P_{CO}$ $k_C = 4.71 \times 10^2 \exp\left(-\frac{109,600}{RT}\right) (\text{kPa}^{-1}\text{s}^{-1})$ $k_{CO} = 3.81 \times 10^{16} \exp\left(-\frac{232,200}{RT}\right) (\text{kmolm}^{-3}\text{kPa}^{-2}\text{s}^{-1})$ $\beta = 2.66 \times 10^4 \exp\left(-\frac{61,500}{RT}\right)$
[43]	✓				1.3–6.1 kPa O_2 partial pressure Charcoal, graphite, coked FCC catalyst	$\frac{CO}{CO_2} = 10^{2.2} x_{O_2}^{-0.64} \exp\left(-\frac{4000 \pm 600}{T}\right)$
[44]	✓				Coked catalyst 320–730 °C	$r_{CO} = k_{CO} C_C C_{O_2}^{0.58 \pm 0.02}$ $r_{CO_2} = k_{CO_2} C_C C_{O_2}^{0.68 \pm 0.02}$ $k_{CO} = (1.1 \pm 0.2) \times 10^6 \exp\left(-\frac{146,000}{RT}\right)$ $k_{CO_2} = (3.0 \pm 0.4) \times 10^3 \exp\left(-\frac{112,000}{RT}\right)$

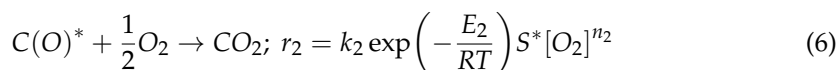
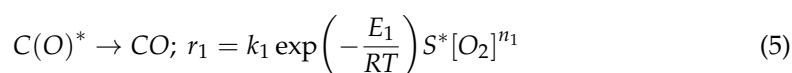
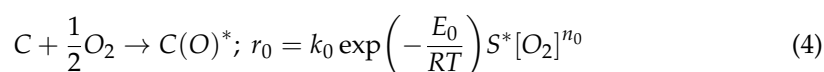
Components: C—coke as carbon, H—coke as hydrogen, CO—Carbon monoxide, CO_2 —carbon dioxide, H_2O —water vapour. Units: P—kPa, T—K, Activation energy—kJ.kmol⁻¹, x (mole fraction)—(-). Reactions: 1—C to CO_2 —C to CO_2 , 3—H to H_2O , 4—CO to CO_2 .

The understanding of the oxidation of carbon monoxide to carbon dioxide is far less straightforward, mostly because it is difficult to measure the concentrations of gaseous products at the surface of the catalyst in the catalyst pores. It is generally accepted that this oxidation occurs both heterogeneously (on the surface of the catalyst) and homogeneously (in the gas phase in the intra particle spaces or pores, and in the bulk gas phase); however, to what extent each of these reactions is significant is not entirely clear. Early workers [45–49] carried out studies towards the development of a global carbon monoxide burnout rate in the gaseous form, in the temperature range 770–2400 K using a variety of fuels such as propane and methane. Although their experiments are not directly on FCC regeneration, they still present a good understanding of the homogenous carbon monoxide oxidation reaction. Experiments were based on combustions of different types of fuel and in vastly different conditions (temperature and pressure ranges), some experiments in the presence of water vapour [49] and others in dry conditions [45,46]. There is general agreement in this literature that oxidation is first order in carbon monoxide. Data across the literature suggest there is some dependency on the temperature in the order with respect to water vapour, with work in the region 770–1500 K [45] seeming to be in support of a half order with respect to water vapour, and those in the range 1500–2400 K reporting lower orders of zero or close to it. There is little agreement in the order of oxygen; Ghazal [50] reported a value of 0.75. Other workers reported different values for the order of oxygen; 0.5 [45] and 0.2 or 1 [49]. Howard et al. [42] collated data from various authors in order to define a global carbon monoxide burning rate, and their results are reported in Table 2. They note that their choices for orders for carbon monoxide and water are because these agree with some of the previously published work. However, they also note that the value for the oxygen order is only chosen because it performs no better or worse than any of the other values reported in the literature. Nevertheless, Howard et al. [42] had confidence in their kinetic rate equation because the data used to produce it were representative of different types of burners, reactors, fuels, equivalence ratios, pressures and temperatures. For the problem of ‘afterburn’ in the FCC unit, data collated by Howard and co seem to suggest their rate equation is sufficient in describing the homogenous oxidation of carbon monoxide. This is because significant deviations from this rate equations were only observed beyond the 1500 K temperature mark, which is beyond the operating temperature for modern FCC regenerators. In this regard, Howard proposed that the mechanism for this reaction can be thought of as an equilibrium reaction involving free radicals of hydroxyl, oxygen and hydrogen. On the other hand, studies conducted to measure this homogenous condition under FCC regeneration conditions [25,41] reported that the overall contribution of this homogenous reaction to the overall carbon monoxide oxidation in the regenerator is negligible. In fact, Tone et al. [25] reported that they found no evidence for this reaction when the reactor is operated at the same temperature and pressure while running carbon monoxide and oxygen stream through the reactor in the absence of the catalyst.

Regarding the catalytic oxidation of carbon monoxide, Tone et al. [25] proposed a reaction mechanism for the regeneration of coked Si–Al cracking catalyst involving the parallel oxidation of carbon in the coke to both carbon oxides, followed by the oxidation of carbon monoxide to carbon dioxide on the surface of the catalyst. They essentially assume that the homogenous oxidation of carbon monoxide is negligible after it was found that the concentration of carbon dioxide in the affluent gas stayed the same when the combustion reactions are conducted without the catalyst present in the reactor. This observation suggested that significant oxidation of CO only occurred in the presence of catalysts particles, meaning only the heterogeneous oxidation is significant to the kinetic study. This result is consistent with the work from Morley and de Lasa [51] which found that of the two oxidations of carbon monoxide, the homogenous reaction was negligible compared to the heterogeneous version. Tone et al. [25] reported the heterogeneous reaction to be first-order in carbon monoxide partial pressure and independent of oxygen partial pressure in the range 0.05–0.15 atm. On the other hand, Arandes et al. [28] also reported rates for this reaction and confirmed that the reaction is first order in carbon monoxide;

however, they reported an order of one with respect to oxygen partial pressure. It is worth noting that the two workers reported similar values for the activation energy of the carbon monoxide reaction, 57.6 kJ/mol [25] and 51.5 ± 0.5 kJ/mol [28]. The small difference is likely due to the variations in the catalyst structure and transition metal composition. It was demonstrated that oxides of transition metals such as copper and nickel promote catalytic carbon monoxide oxidation [25]. This variability brought about by transition metal oxides inevitably means that the rate equations and kinetic constants for this reaction will vary across different studies, and therefore, it is difficult to produce a universal rate equation for the FCC regeneration as FCC catalysts are widely different in their transition metal content. The same problem is encountered when dealing with the rate equations for coke combustion, as it was also shown that transition metals on the catalyst or in the coke could catalyse the reaction to varying degrees [26].

Thus far, the kinetic studies discussed only involved models that describe the overall conversion of coke to gaseous oxides without regard for the mechanism involved in the conversions or the reaction intermediates. Several workers studied the rate of combustion of unsaturated coke on FCC catalyst by explicitly including the carbon oxide complexes formed on the catalyst surface in the reaction mechanism. These ‘surface complexes’ can then transform to produce CO or CO₂. Generally, two types of such studies exist in the literature [44]: the first is such that direct conversion of coke and oxygen to form surface complexes, and the second uses the Langmuir-type model for dissociative adsorption. The type of model used determines the forms of the rate equations. In the first case, the chemical and rate equations (shown in Equations (4)–(6) may be written as follows [44]:



where S^* is the molar amount of surface intermediate complex, $C(O)^*$, and n is the reaction order with respect to oxygen concentration. Equations (4)–(6) show one suggested mechanism for oxidation; however, the exact mechanism has been debated for years in the literature. Some of the main issues of contention are the formation, or lack thereof, of $C(O_2)^*$ complex and whether or not the carbon oxides (CO and CO₂) are formed as primary products of coke combustion [43]. As a result, many workers developed kinetic models that show alternative mechanisms for this coke oxidation reaction [43,52,53]. In the Langmuir-type model, Equation (4) to form the carbon oxide complex is replaced by an equilibrium reaction shown Equation (7), while the other reactions remain unchanged [44]:



r_1 and r_2 (Equations (8) and (9), respectively), which are the rate equations for the formation of CO and CO₂, respectively, can be written in the following forms [44]:

$$r_1 = \frac{k_1 \exp\left(-\frac{E_1}{RT}\right) \left[k_0 \exp\left(-\frac{\Delta H}{RT}\right) [O_2] \right]^{\frac{1}{2}} S^*}{1 + \left[k_0 \exp\left(-\frac{\Delta H}{RT}\right) [O_2] \right]^{\frac{1}{2}}} \quad (8)$$

$$r_2 = \frac{k_2 \exp\left(-\frac{E_2}{RT}\right) \left[k_0 \exp\left(-\frac{\Delta H}{RT}\right) [O_2] \right]^{\frac{1}{2}} S^* [O_2]^{n_2}}{1 + \left[k_0 \exp\left(-\frac{\Delta H}{RT}\right) [O_2] \right]^{\frac{1}{2}}} \quad (9)$$

where ΔH is the adsorption enthalpy, and everything else is as defined previously. These two models described here have the advantage of incorporating the effect of adsorption explicitly at the surface to the rate of oxidation, but this comes at the cost of an increase in the number of parameters being estimated from experimental data. Kanervo et al. [44] applied all three models described here to kinetic studies of spent FCC catalyst regeneration. They found that all three models adequately described the coke oxidation experimental data well, meaning no considerable advantage is gained from explicitly including the surface complexes into the reaction scheme. This result also meant it was difficult to ascertain which mechanism accurately described the system definitively; hence, this remains an open question. However, for the purposes of FCC regenerator modelling, researchers seldom use kinetic models that describe the formation of surface complexes, opting instead for the simpler model described in Equations (1)–(3), which capture all the necessary information without losing much accuracy.

Table 2 summarises some kinetic studies that are relevant to the modelling of the FCC unit regenerator. In conclusion, the literature of kinetic studies related to the regenerator is vast, and the main reactions occurring in the unit are well known. Generally, coke is understood to be a complex mixture of carbon and hydrogen, based on its hydrocarbon origins, with varying H/C ratios depending on feed. The coke combustion reaction is generally believed to follow simple first-order kinetics with respect to both carbon and hydrogen and with respect to oxygen. Carbon monoxide formed proceeds to be oxidised to carbon dioxide both homogeneously and heterogeneously, but there is some debate over which of the two carbon monoxide reactions is more important to the conversions of the unit. Therefore, for completeness, both reactions can be used in the model. It is difficult to compare various kinetic studies on regenerator reactions because some metals may catalyse the reactions, and their varied composition in FCC catalysts results in varied kinetic parameters. The rich literature in this area means that researchers are spoilt for choice when it comes to choosing a kinetic scheme and kinetic parameters for their regenerator model. However, it is important that the choice be based on the range of operating conditions in which the kinetic model is valid and on the type of catalysts that are used in the study since how well kinetic parameters extrapolate beyond their range of validity is not known, and the effect of catalyst variations was already described.

2.2. Hydrodynamics of the Regenerator

2.2.1. Axial Profiles

Experimental data of axial profiles of solid holdup in an FCC regenerator from Kim and Kim [3] are shown in Figure 1. The profile resembles an ‘S-shape’ profile with three visible regions: (a) the region near the distributor which has a high volume of solid, (b) the region at the top which has a small volume of solid, and (c) the short transition region in between. The difference in the solid holdup between the top and the bottom of the bed creates two discernible regions in the bed. The dense bed, region (a), consists of most of the solids and gases, and the freeboard (or lean phase), region (b), consists of the gas leaving the bed and the small fraction of solid particles entrained in that gas. Gases and particles leaving the freeboard region are separated in the cycles at the top of the regenerator, where catalysts are returned to the dense bed while the gas can leave the regenerator chamber. Since the dense bed region is the region containing most of the solids and gas, it is generally accepted that this is where most of the combustion of coke on catalyst takes place. For modelling purposes, an understanding of the mixing and flow behaviour inside the dense bed is required.

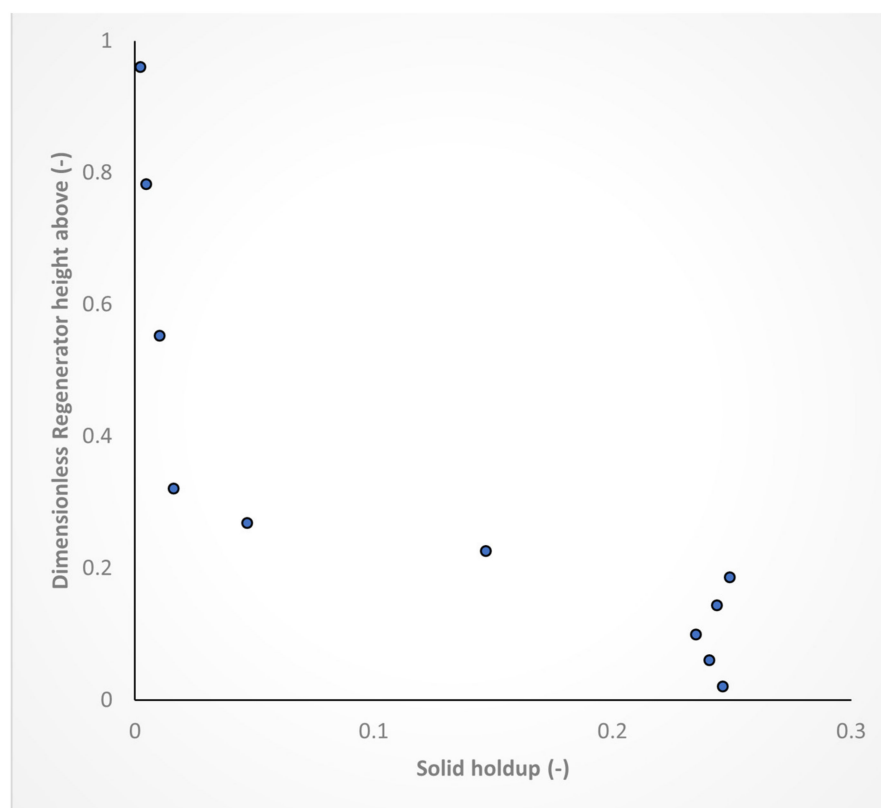


Figure 1. Axial solid profile in FCC regenerator (redrawn from [3]).

2.2.2. Bubbling Behaviour

The FCC regenerator at normal operation with modern FCC catalyst particles is known to occur in the bubbling/turbulent regime of solid–gas fluidisation [3]. The fluidisation behaviour is known to be dependent on the physical properties of the solid particles, such as size and density. Geldart and co-workers [54,55] provided a classification of particles based on their fluidisation behaviour; this classification is the most widely used in the field of gas–solid fluidisation. The FCC catalyst is classified as Group A particles [11,56]. This classification means that these particles are characterised by relatively small particle size ($30 \leq d_p \leq 150 \mu\text{m}$). These particles easily form bubbles that rise at velocities higher than the emulsion gas velocity when fluidised. For group A particles, two velocities are of significance in the bubbling bed region: U_{mf} , the minimum fluidisation velocity, and U_{mb} , the minimum bubbling velocity. Determination of minimum fluidisation is generally trivial, starting from a fixed bed of particles in a vessel with a porous base to allow the fluidising gas to be pumped through the bed; the velocity of the gas is then increased until incipient fluidisation occurs. The literature on the derivation of correlations for minimum fluidisation velocity is vast [57–64]. Usually, correlations of U_{mf} are derived by dimensional analysis involving fluid dynamics dimensionless numbers such as drag coefficient, Reynold’s number, Galilei number, Archimedes number related by to flow and particle properties such as densities and particle size. The U_{mf} literature is reviewed and summarised elsewhere [65,66]. Several authors also provided correlations to describe the transition of Group A powders at the minimum bubbling velocity [55,67–70]. The study of the behaviour of bubbles formed in fluidised bed (beyond U_{mb}) has been of great interest to many researchers. These studies produced great insights into gas–solid flow in FCC regenerators during normal operation.

Additionally, evidence of the formation of bubbles in the dense bed in the regime beyond U_{mb} is seen from the X-ray studies [71–75]. Bubbles here refer to the voids or pockets of air that are observed rising through the surrounding gas–solid emulsion. Studies that focus on the movement of isolated bubbles are usually the starting point in the

understanding of bubble motion in the dense bed. These studies are divided into two: (i) two-dimensional beds (formed from two thinly separated parallel-sided transparent plates) and three-dimensional beds. Bubbles in two-dimensional beds were observed to be shaped like spherical caps, while bubbles in three-dimensional beds appear spherical with indented bases [56]. Both studies show bubbles rising through the emulsion before eventually erupting at the surface of the dense bed. This observation is important for modelling because it establishes the inherent heterogeneity that is found in the dense bed for a freely bubbling bed operating beyond U_{mb} , so that this dense bed region can be thought of as being made up of two distinct phases. Consequently, the famous two-phase theory by Toomey and Johnstone [13] of fluidisation was developed to describe this observed flow behavior, and it postulated that the two regions are the emulsion, which is the continuous phase where the solid particles are found, and the bubble phase, which is essentially a solid free void containing gas. According to this theory, the emulsion is static at incipient fluidisation conditions while any gas in excess of that required for minimum fluidisation travels through the bed in the form of bubbles. The theory provided a framework for mathematically describing the flow in bubbling/turbulent beds and has been widely used in the modelling of gas–solid beds in this regime, including the FCC regenerator. Furthermore, the tracer experiments of Rowe [76] provided great insights into the flow around the rising bubble phase, showing a region of penetration of bubble gas into the emulsion; this region is seen around the rising bubble and is clearly discernible from the bubble and the emulsion phases. The distinct nature of this region meant it was hydrodynamically different from the two phases described by the two-phase theory. This region was termed the cloud. Additionally, these tracer experiments also showed that the indented base of the bubbles is filled with a cluster or conglomerate of particles that are drawn by the bubbles as they rise to the surface. This mechanism of particles being drawn by rising bubbles, as is described later, has been identified as the prime mechanism for solid mixing in the bed [65]. This leads to the conclusion that an extra phase can be identified (i.e., the cloud and wake phase) between the emulsion and the bubble, an observation that led to the bubbling bed model by Kunii and Levenspiel [15]. Unlike in gas–liquid systems where the interphase is a continuous film surrounding the bubble, no such film exists in gas–solid systems. Bubbles are prevented from collapsing by pressure exerted on the particles by enclosed gas; however, the interphase is permeable to gas [56]. The significance of this observation for heterogeneous systems such as combustion of coke on the catalyst in the regenerator is that gas in the bubble is not in contact with the solid or catalyst particles meaning bubbles may lead to a significant bypass of gas. The transport of gas such as oxygen from within the bubbles to the emulsion encounters resistance through the cloud–wake region on both sides, i.e., at the interphase with the emulsion and with the bubble. Therefore, under certain conditions, such as high superficial gas velocity, bypass is a likely phenomenon [56].

The velocity and size of the rising bubble are important parameters when modelling the dense bed because, as was explained above, the large velocity of bubbles may result in poor gas–solid contact and bypassing. Photographic studies of rising bubbles are quite clear that bubbles are seen rising, and their size changes as they rise [77]. Two processes, which occur in parallel for any freely bubbling bed, are responsible for the change in the size of bubbles as they rise: (i) coalescence and (ii) bubble splitting. Coalescence is identified as the main reason for bubble growth, the other being that the decrease in hydrostatic pressure with height above the base of the dense bed; however, the effect of hydrostatic pressure is assumed insignificant compared to coalescence [78]. Coalescence is a nucleation process that occurs when two bubbles merge with one another to produce a bigger bubble, and it was observed in two-dimensional beds. Evidence of coalescence in freely bubbling beds is seen through the existence of two different bubble profiles at the top and bottom of the dense bed; the top consists of a small number of relatively large bubbles, whereas at the bottom of the dense bed, a large number of small bubbles is observed [56]. This suggests that bubbles merge and grow as they rise. From this observation, several studies were carried to correlate the size of the bubble to some operating parameters, such as the height

of the bed above the distributor plate [71,77,79–85]. On the other hand, Rowe [86] observed rising bubbles developing cusps on the roof and then subsequently splitting to form two smaller bubbles. Usually, the smaller of the two bubbles are seen being reabsorbed, but in some instances, especially for fine particles (diameter < 45 µm), the two bubbles then continue to rise separately [11]. As a result of both the growth and splitting of bubbles occurring simultaneously in the bed, Davidson and Harrison [87,88] theorised that there must exist a limit on the size of the growing bubbles inside the bed. Basically, for a given bed and flow conditions, bubbles rising in the bed will not grow past a particular size. This theory is based on the assumption that as a bubble rises, the drag exerted by particles moving downward relative to the bubble (in the surrounding cloud and emulsion phases) sets in motion internal circulation currents of the gas within the bubble, and that velocity of said circulation, U_c , approximates the bubble rise velocity, U_b . As U_c ($\sim U_b$) increases, due to coalescence, such that $U_c > U_t$ (where U_t is the terminal fall velocity of the particles in the bed), then the solids in the wake are drawn up inside the bubble resulting in splitting. Therefore, the limit on the bubble size is reached when d_b corresponding to bubble rise velocity equal to U_t is reached. An alternative theory to bubble splitting states that the breakage of bubbles is primarily a result of the development of instabilities at the roof of the bubble, allowing particles ahead of the bubble to fall through the void and divide it into two [89–91]. It is not exactly clear in the literature which of these theories is correct, but it is deducible that the likely reason for splitting is the entry of solid particles into the bubble and that the best predictor of whether or not this occurs is the velocity of the rising bubble. Since U_b is connected to d_b [92], these two properties of the bubble have been correlated in experiments [72,73] so that bubble splitting can be predicted from bubble rise velocity.

Davidson and Harrison [88] drew similarities in the rise of air bubbles in liquid systems to that of gas bubbles in gas–solid systems. They found that the famous [93] correlation in Equation (10) for rising air bubbles in gas–liquid fluid beds predicted the U_b of an isolated bubble in gas–solid systems reasonably well. The reason why this equation is valid for solid systems is not clear.

$$U_b = 0.711\sqrt{gd_b} \quad (10)$$

Sit and Grace [94] studied oxygen gas bubbles in two-dimensional beds and found that bubbles in proximity affect each other's rise velocities. They found that during the process of coalescence, the trailing bubble in a pair accelerates towards the leading bubble until the encroachment period. It is clear from this that the rise velocity of a swarm of bubbles in a freely bubbling bed will be different from that given by Equation (10). Davidson and Harrison [88] then proposed a theory that the average velocity of a bubble in a freely bubbling bed is the sum of the velocity the bubble would have rising in isolation, see Equation (10), plus the upward velocity of the particulate phase between the bubbles. This is summarised in Equation (11).

$$U_b = 0.711\sqrt{gd_p} + (U - U_{mf}) \quad (11)$$

Equation (11) is widely used in reactor modelling and design [11]; however, its validity has been questioned [84]. Other similar equations for bubble velocity in freely bubbling beds were proposed by various workers [95–97]; however, there is little agreement between them [56]. As a result, it is usually sufficient, at least in the initial stages of design, to use Equation (11) for bubble rise velocity. Where a correlation for bubble size with bed height is available, Equation (11) then gives the variation in the velocity of the bubbles in a swarm with the height of the bed. Equations (10) and (11) show that the rise velocity of the bubbles, either in isolation or in a freely bubbling bed, is correlated to the size of the bubble, hence the multitudes of studies that have been devoted to producing these correlations for different process conditions [92].

The issue of solid and gas mixing in the dense bed is also of significance, especially for the purposes of modelling. Rowe [86] in Figure 2 showed the displacement caused by the passage of a single bubble. Originally the bed contained two differently coloured

materials of equal size and density profiles; the coloured substance originally occupied only the bottom of the bed, with the white particles occupying the top. Rowe [86] reported that the bed became fully mixed after the passage of 50 bubbles. Rowe and Partridge [72,73,76] described two mechanisms as being responsible for this solid mixing behaviour in the dense bed. Firstly, solids are carried in the wake of the bubble and subsequently ejected at the surface of the bed and replaced by emulsion solids. Secondly, the drift mechanism of bubbles draws up solids as they rise, leaving behind a finger of underlying material (as seen in Figure 2). These two-mechanism are described as being the main mechanisms in which particles move large distances in the dense bed and therefore inducing mixing. Several other workers [98–102] all reported similar behaviour, with particles seen to be moving upwards in areas of rising bubbles and downwards in areas of low bubbling. Stein et al. [100] used positron emission particle tracing and a three-dimensional bed to observe particle trajectories. They observed that particles move upward in the central region of the bed (where most bubbling occurs) and downwards near the wall. This is consistent with the radial bubble flow profiles reported by Werther and Molerus [103] that showed high bubble flow in the central area of the bed and none at or near the walls. As a result of this motion, good axial mixing of solids can be assumed. In contrast, evidence of poor lateral mixing of solids was presented by Callcott et al. [104] using a rectangular bed. Poor lateral/radial mixing of solids was also demonstrated through small lateral/radial solid dispersion coefficients compared to the axial direction [105–108]. Callcott et al. [104] found that solid tracers could be completely mixed vertically in 75 s at a fluidisation velocity of $3U_{mf}$, but complete mixing over the horizontal direction required about 1.5 h. The upward motion in the centre and downward motion at the walls result in a circulation pattern that is often referred to as a ‘Gulf Stream’ circulation. This ‘Gulf stream’ circulation of particles can be influenced by flow nonuniformity at the distributor plate [109]. Differences in gas distribution systems of industrial units mean that each unit can have its own preferred flow paths, and therefore its own solid circulation and mixing characteristics. In summary, for solids in the dense bed, axial mixing of solids is usually good enough that well-mixed assumption in this direction is reasonable. However, this assumption may break down when considering mixing in the lateral direction. The significance of this is that poor lateral mixing may result in the creation of hotspots in the reactor along the radial direction. Because most models that are 1-D are essentially averaged across the reactor area, they are unable to predict these hotspots and therefore may lead to inaccurate predictions.

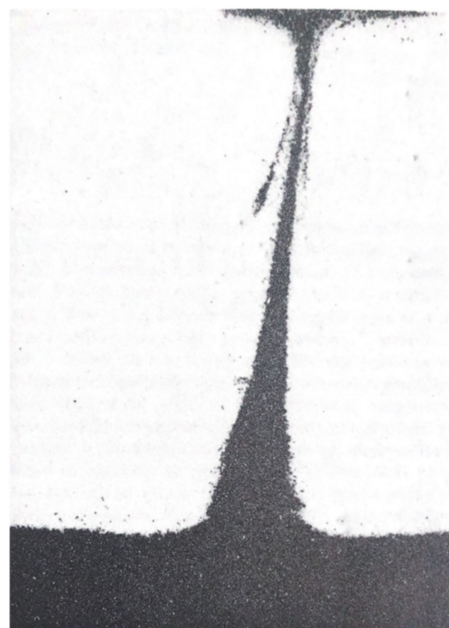


Figure 2. Displacement caused by a single rising bubble through a three-dimensional bed [86].

2.3. Reactor Models for Bubbling Beds

Grace [110] emphasised the importance of the hydrodynamic factors (such as gas distribution, bubble size, residence time distribution, phase division and interphase exchange, etc.) and kinetic factors (such as stoichiometry, reaction orders and kinetic constants, etc.) to modelling of reactors. In order to predict the contact and flow inside the FCC regenerator, the development of a model to describe the flow is required. Several classifications for hydrodynamic models of fluidised beds exist in the literature. The famous classification is by Harris and Davidson [111], who classify models into three categories, i.e., (i) models that predict the radial variation in solid suspension but not axial, (ii) models that predict axial solid suspension but not radial and (iii) models that employ fundamental fluid dynamic equations for two-phase gas–solid flow. Yates [56] classified models as (i) simple or arbitrary models based on empirical correlations obtained from small-scale experiments and (ii) models based on bubble dynamics that describe reactor behaviour in terms of the known physics and hydrodynamics of fluid beds. Ultimately model classification is difficult because the objectives of the classifications differ, and there is so much overlap that it becomes a strenuous task to group them. For the present work, the classification by Yang [78] based on phase description is employed. This is chosen here because this classification is straightforward as balance equations are developed for each phase without having to worry about what happens within the same phase. Phase description allows mass, energy and momentum balances for each phase assumed present in the reactor to be carried out, and therefore, the behaviour of properties of each phase can be predicted. By this classification, three classes of models are identified; (i) homogeneous models, two-phase models and three-phase/bubbling bed models. An extra class is discussed where the phases in some regions cannot be assumed to be consistent with phases in the rest of the dense bed.

The primary postulate of two-phase models is their treatment of gas division among the two phases. As mentioned before, traditionally, it was assumed that all gas in excess of that required for minimum fluidisation passed through the bed in the form of bubbles. However, several investigators found that this assumption greatly overestimates the so-called visible gas flow (or flow through the bed in bubble form) and underestimates the flow of gas in the emulsion [71,112–114]. Rowe [115] showed that higher conversion is achieved than predicted by conventional two-phase theory as a result of higher than predicted interstitial gas flow. As a result, corrections are usually employed to account for this deviation from the ideal two-phase flow. The commonly used corrections are in the form [112] as seen in Equations (12) and (13):

$$\varepsilon_b U_b = Y(U - U_{mf}) \quad (12)$$

$$U_b = (U - U_b)(1 + k\varepsilon_b) \quad (13)$$

where Y and k represent the deviation from the ideal two-phase flow. The primary difference between bubble velocity predicted by Equations (12) and (13) to that predicted by correlations such as that shown in Equation (11) is that the former only predicts bubble velocity using U_{mf} and makes no reference to bubble size. It is reasonable to assume that the latter would be more representative of the real system as they are capable of predicting acceleration caused by bubble growth. Nevertheless, both types of correlations have been used in modelling bubbling beds in the literature.

One of the earliest two-phase models was by Davidson and Harrison [88]. It made the following assumptions: (a) gas in emulsion at U_{mf} and is either well mixed or plug flow, (b) bubbles exist through the bed with uniform size and (c) interphase gas exchange is by diffusion and through flow between emulsion and bubbles. Although this model agreed well with some experimental data, it has been criticised for its simplistic definition of the gas–solid bubble and was later updated by other workers [56,116] to account for bubble growth in beds of fine particles. Since then, more work has been published using this model to account for axial gas dispersion.

Kunii and Levenspiel's [15] bubbling bed model is one of the earliest incorporations of the cloud and wake region. The assumptions of this model are: (a) most reactant gas travels up the bed in uniform size bubbles surrounded by cloud and wake, and interstitial gas flow is negligibly small in comparison, (b) plug flow in bubble phase, and (c) interchange between emulsion and bubble phase is through the cloud and wake, through two resistances to transport. As with the previous model, many variations in the bubbling bed model now exist in the literature to account for such things as the gas flow through the emulsion, the growth of bubbles up the bed and the dispersion of gas up the reactor. Such models include Stephens et al.'s [16] counter-current back mixing model, which updated the bubbling bed model by including emulsion phase back mixing, downflow of solids during circulation and linear increase in bubble diameter. Kato and Wen's [17] model updated the bubbling bed model by assuming bubble size growth is given by a correlation and that bubble and emulsion phases in the bed are represented by a series of well-mixed tanks whose heights are equal to the bubble diameter corresponding to that vertical position above the distributor.

Grid enhanced models vary from the above models in that the region near the distributor is considered to show a different flow pattern to the rest of the bed. It is assumed gas penetrates the bed in the form of jets [117]. Photographic studies of the grid region showed that the term 'jet' refers to a variety of flow patterns near the gas inlet, such as elongated cavities forming above the orifice and leaving as bubbles [118], plumes developing necks which divide into a series of bubbles [119], chains of bubbles emanating from the orifice [120] and permanent flame-like dilute phase regions penetrating into the bed [121]. In their model, Behie and Kehoe [117] made no distinction between these flow patterns and assumed that these jets could generally be taken as plug flow in the axial direction and perfectly mixed radially/laterally. The jetting effect is thought to produce enough turbulence in its vicinity that the phase surrounding the jet is assumed to be a well-mixed emulsion. Of course, some variations to this jet transport model near the grid exist, for example, the tubular jet model [122] and the sink and source model [123,124]. The jet penetration height (referred to as h in Table 3) was also studied in detail and correlations exist to find it. Davidson et al. [65] reviewed and published some of this literature in their book.

In the general case, the energy balance for the system (in Equations (14) and (15) could be written for each phase, assuming a two-phase flow model:

Bubble phase:

$$\rho_b \frac{\partial(\varepsilon_b h_b)}{\partial t} + \rho_b \frac{\partial(\varepsilon_b U_b h_b)}{\partial z} = \Delta Q_{reaction} + \Delta Q_{be} + S_b \quad (14)$$

Emulsion phase (for a well-mixed emulsion with thermodynamic equilibrium):

$$\rho_b \frac{\partial(\varepsilon_e h_e)}{\partial t} = \Delta Q_{reaction} + \Delta Q_{eb} + S_e \quad (15)$$

where the ε_b and ε_e are volume fractions of the bubble and emulsion, respectively, h_b and h_e are the specific enthalpies of the bubble and emulsion phases, respectively, $\Delta Q_{reaction}$ is the heat of reaction in the phase which depends on the rates of reactions and their associated heats of reaction, ΔQ_{be} and ΔQ_{eb} are the heat exchanges between the bubble and emulsion phases, respectively, which depend on the heat transfer coefficient between the two phases, the interphase area and the temperature difference between the phases. S_b and S_e are the energy source/sink terms in the bubble and emulsion phases, respectively.

Table 3. Classification of reactor hydrodynamic models for FCC regenerator type Fluidised beds.

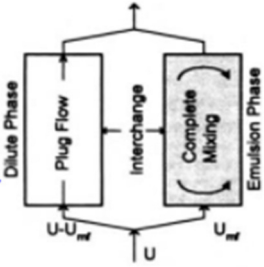
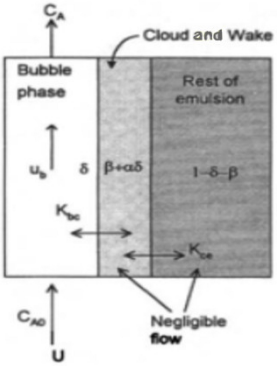
Model Classification	Description	Governing Mass Balance Equations
<p>Two-Phase Flow Models Two-Phase Flow Models</p> 	<p>This model was first proposed by Toomey and Johnstone [13]. It draws from the observations of bubbles rising in bubbling beds and postulates that two phases in the bed exist, i.e., the emulsion and the bubble phase. According to the original theory from Toomey and Johnstone, the emulsion phase is at minimum fluidisation conditions while any gas through the distributor plate in excess of that required for incipient fluidisation passes through the bed in the form of bubbles (i.e., the bubble phase). Each phase is represented by a mass balance equation, and an interchange term is included in each equation for transfer between the phases. If more than one component is present in the phase, i.e., a mixture of gas in air bubbles, separate equations are written for each phase.</p> <p>Generally, gas flow in the bubbles is assumed to be plug flow, while gas flow in the emulsion is assumed plug flow or well-mixed [78]. However, non-ideality of flow in dense beds is likely, so models can replace traditional ideal flow with dispersion models, tanks in series and residence time distribution models.</p>	<p>For emulsion gas: $\frac{\partial C_{Ae}}{\partial t} - D_{Ae} \frac{\partial^2 C_{Ae}}{\partial z^2} + U_e \frac{\partial C_{Ae}}{\partial z} + K_{be}(C_{Ae} - C_{Ab}) + R_{Ae} = 0;$ For bubble phase: $\frac{\partial C_{Ab}}{\partial t} - D_{Ab} \frac{\partial^2 C_{Ab}}{\partial z^2} + U_e \frac{\partial C_{Ab}}{\partial z} + K_{be}(C_{Ab} - C_{Ae}) + R_{Ab} = 0;$ For plug flow $D_A = 0$, and for well-mixed flow $D_A = \infty$, for dispersion model D_A is defined.</p>
<p>Bubbling bed Models or Cloud and Wake Models</p> 	<p>These models are an extension of the two-phase models. They were first proposed by Kunii and Levenspiel [15,125,126] to account for the cloud and wake regions that were seen from X-ray imaging studies [72,73]. This consideration of the cloud-wake phase adds extra resistance to mass and heat transfer between the emulsion and the bubble phase. There is bubble→cloud resistance and cloud → emulsion resistance. These models are usually governed by these assumptions: (a) bubbles are uniform in size and evenly distributed, (b) flow in the vicinity of the bubble follows the Davidson [88] model and (c) emulsion stays at minimum fluidisation velocity.</p>	<p>Assuming flow through the bed only in the bubble phase (reasonable at high gas superficial velocities), mass balance equations are as follows [78].</p> <p>Bubble phase: $-\frac{1}{V_b} \left(\frac{dN_{Ab}}{dt} \right) = R_{Ab} + K_{bc}(C_{Ab} - C_{Ac});$ Cloud-wake phase: $K_{bc}(C_{Ab} - C_{Ac}) = R_{Ac} + K_{ce}(C_{Ac} - C_{Ae});$ Emulsion phase: $K_{ce}(C_{Ac} - C_{Ae}) = R_{Ae};$</p>

Table 3. Cont.

Model Classification	Description	Governing Mass Balance Equations
Multiple Region Models	<p>These models differentiate between different regions in the regenerator dense bed; for example, it was described above that imaging studies showed that bubbling behaviour in the region near the gas distributor plate (large number of small bubbles observed) is different from the behaviour at the top of the dense bed (small number of large bubbles observed). Furthermore, it was also observed that changing only the gas distribution plate in a reaction system leads to different conversions in the reactor [117,127]. This evidence led Behie and Kehoe [117] to propose the Grid effect model, which treats the region of the bed near the distributor plate differently from the rest of the dense bed. From this proposition, the grid region may be modelled differently, while either one of the previous models is used to describe the rest of the bed, with jets assumed to lose momentum and break off into bubbles [65]. According to the original model from Behie and Kehoe, gas enters the bed through the distributor in the form of high-speed jets that penetrate the emulsion to a distance h before bubble formation is observed. This region between the distributor and the part of the bed up to h is considered the grid region. Jets are assumed to cause turbulent mixing of the emulsion, and hence emulsion is assumed perfectly mixed, while the jets are assumed perfectly mixed laterally/radially and plug flow in the axial direction.</p>	<p>For the grid region, i.e., $0 \leq z \leq h$ at steady state.</p> <p>Gas in the jets:</p> $U_j \frac{\partial C_{Aj}}{\partial z} + K_{je} (C_{Aj} - C_{Ae}) = 0;$ <p>Gas in the emulsion:</p> $U_e (C_{Ae0} - C_{Ae}) + \int_0^h K_{je} (C_{Aj} - C_{Ae}) dz + R_{Ae} = 0;$ <p>This model predicts that the transfer coefficient K_{je} is 40–60 times the value of the coefficient between bubble and emulsion phase (i.e., K_{be}) [78]. This result is expected since the bubble formation profile near the grid is shown to favour more turbulence (and therefore better mass transfer) in this region than in the rest of the dense bed.</p>

The other class of hydrodynamic reactor models not included in Table 3 are the pseudo-homogenous models that make no distinction between the emulsion phase and the bubbles passing through it. These models, therefore, do not have any division of gas in the dense bed and often employ simple mixing models such as plug flow, well-mixed tanks, tanks in series and dispersion models for gases and solids mixing in the bed [78]. Ultimately, within this framework of model classes, there is a lot of flexibility in that simulation engineers have the ability to choose between different alternative assumptions for (i) phase description in the dense bed (i.e., emulsion–bubble, emulsion–cloud–bubble or pseudo-homogenous), (ii) mixing characteristics for gases and solids in the bed (i.e., plug flow or well-mixed or dispersion model) and (iii) the heat and mass transfer resistance between phases (i.e., direct transfer between emulsion and bubble, or transfer between emulsion and bubble via cloud phase). This flexibility has inevitably resulted in a wide variety of unique models for modelling bubbling bed reactors in the industry. Table 4 shows a review of FCC regenerator models published between 1990 and 2020 in terms of kinetic modelling and hydrodynamics described in this work. We have attempted to summarise the variety of model assumptions in Figure 3 based on the review in Table 4. Generally, it can be seen that the model complexity of bubbling/turbulent beds with significant bubbling activity is based upon the distinct phases present in the bed. For two-phase models, the gas division is an important parameter since it determines the flow rate of gas through the two phases. Clearly, the two-phase model in its original postulates has proven inadequate in the prediction of gas division, but it is nevertheless a good starting point for most bed designs. Another consideration for some beds is the existence of different regions in dense beds, with the region near the distributor having some obvious hydrodynamic differences from the rest of the bed, hence requiring separate treatment in the model. However, this effect is usually negligible except in shallow beds. The simplest models will ignore the existence of different phases and regions in the bed, assuming pseudo-homogeneous flow in the reactor, although the current literature suggests these models have been phased out as they fail to predict the heterogeneity that is important to reactor performance.

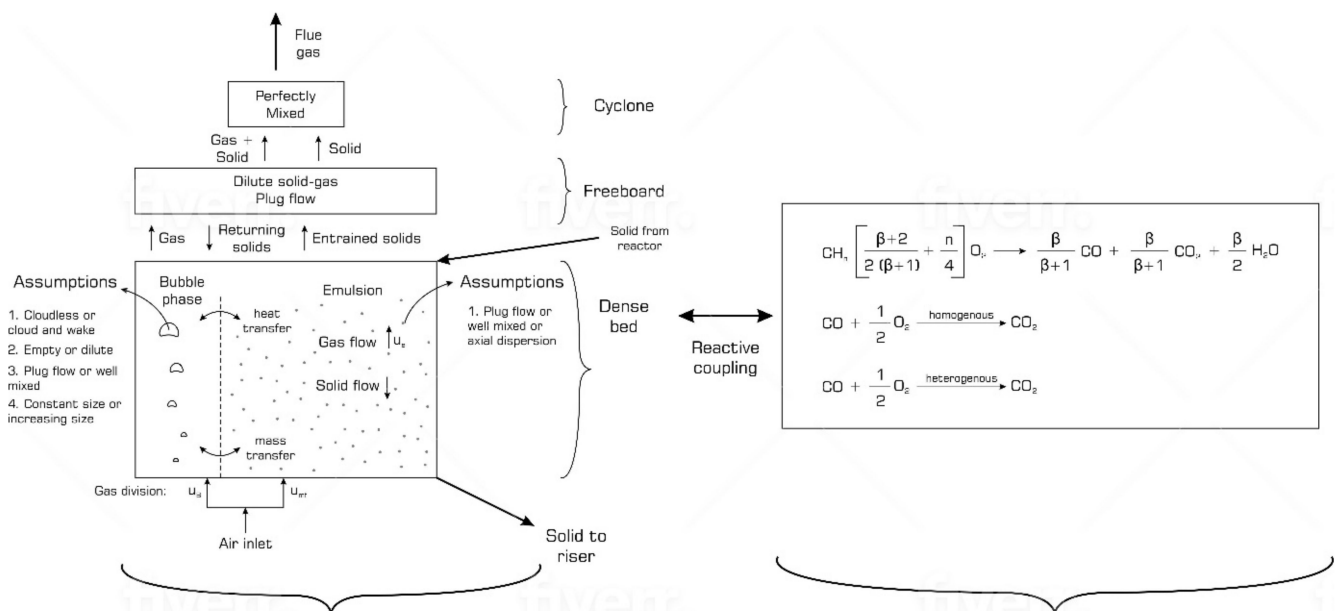


Figure 3. Summary of Regenerator modelling and key hydrodynamic assumptions.

It is shown in Table 4 that the description of coke used in the FCC regenerator is that of coke modelled as pure carbon, or coke modelled as a hydrocarbon mixture with empirical formula CH_q , where q is the molar ratio of hydrogen to carbon, ranging from 0.4 to 2.0, as shown by Hashimoto et al. [39].

Table 4. Review of FCC Regenerator models.

Investigators	Dense Bed						Freeboard	
	Kinetic Model Description		Hydrodynamic Model Description				Kinetic	Hydrodynamic
	Coke Definition	Reaction Rates	Model Class	Emulsion	Bubble			
[36]	C	Coke burning by Kunii and Levenspiel [14]. No bubble phase reaction.	Two-phase	Perfectly mixed emulsion for both solids and gases.	Bubble phase is plug flow.	N/A	N/A	
[128]	$CH_{0.7}$	Complete and Incomplete coke burning kinetics from de Lasa and Errazu [129,130]. CO oxidation ignored.	Grid effect model with two-phase dense bed.	Well-mixed emulsion for solids and gases.	Well-mixed bubble phase. Single uniform value of bubble size defined.	N/A	N/A	
[131]	CH_n $0.83 \leq n \leq 1.67$	Complete and incomplete C burning, H burning, homogenous and heterogeneous oxidation of CO with kinetics from Faltsi-Saravelou and Vasalos [132].	Grid effect model with a Two-phase bubbling region. Grid region has a fully mixed zone and a dead zone in series.	Well-mixed emulsion for both solids and gases.	Plug flow bubble phase. Bubble size not defined.	N/A	N/A	
[19]	C	Coke burning, homogeneous and heterogeneous CO oxidation kinetics as defined by [41,51].	Two-phase	Well-mixed emulsion for both solids and gases.	Plug flow bubble phase.	N/A	N/A	
[10,18]	CH_n	Studies [22–24] for coke combustion. Study [26] for homogenous CO oxidation. [133] for heterogeneous CO oxidation.	Two-Phase	Well-mixed solids. Tubular reactor for gases.	Tubular reactor for bubble phase. Used [11] correlation for bubble size with axial level.	Only homogenous afterburn considered.	Two-phase tubular reactor.	
[134]	CH_n n not defined	Complete and incomplete coke burning, homogeneous and heterogeneous CO oxidation with kinetics as defined by [1].	Two-phase	Well mixed for both solids and gases.	Bubble is well mixed. Bubble size not defined.	All dense bed reactions considered.	Plug flow for both solids and gases.	

Table 4. Cont.

Investigators	Dense Bed						Freeboard	
	Kinetic Model Description		Hydrodynamic Model Description				Kinetic	Hydrodynamic
	Coke Definition	Reaction Rates	Model Class	Emulsion	Bubble			
[135]	$CH_{0,8}$	Carbon burning and CO heterogeneous combustion kinetics by [136]. Hydrogen burning kinetics by [27]. Homogenous CO oxidation kinetics by [137].	Pseudo-homogeneous	Well-mixed tanks for both solids and gases in each of the R2R regenerators.	N/A	N/A	N/A	
[138]	C	Coke burning and CO oxidation kinetics from [41].	Two-phase	Well-mixed emulsion for both solids and gases.	Bubble phase is plug flow. Bubble size not defined.	N/A	N/A	
[139]	$CH_{1,18}$	Complete and incomplete coke burning, homogeneous and heterogeneous CO oxidation all considered, but kinetics source not clearly stated.	Pseudo-homogeneous	Phase is well mixed for solids. Gases in plug flow.	N/A	All dense bed reactions considered.	Plug flow for both solids and gases.	
[20]	CH_n	Reaction scheme as defined by [10,18].	Two-phase	Well mixed for solids. Plug flow for gases.	Plug flow for bubble phase.	All dense bed reactions considered.	Not defined explicitly.	
[140]	C	Coke combustion, homogenous and heterogeneous oxidation as defined by [1].	Pseudo-homogenous	Well-mixed phase for both solids and gases.	N/A	Only homogenous afterburn considered.	Plug flow for gases. No catalyst in freeboard.	

Although the homogenous carbon monoxide oxidation was generally found to be negligible compared to the heterogeneous version, such as in the work of Morley and de Lasa [51], both reactions were included in models of the FCC regenerators to varying degrees. This allows models to be subdivided into three categories with respect to CO oxidation: (i) models that consider only the heterogeneous reaction [138], (ii) models that consider only the homogenous reaction and (iii) models that consider both reactions [1,10,140]. Models that ignore the post-combustion CO oxidation reactions completely, such as [36], were generally phased out, which shows the significance of these so-called afterburn reactions. Ultimately, the level of detail included in the kinetic model depends on the end-use of the model and the accuracy required. In recent times, with stricter regulations surrounding emissions, it is advisable to include all the important reactions so that more accurate predictions of emissions can be made.

Models increase in complexity from homogeneous to two-phase models to grid effect models. Table 4 shows that the simple pseudo-homogeneous models are seldom used to model FCC regenerators. One reason for this is that pseudo homogeneity in fluidised beds is usually observed at a smooth fluidisation regime, and the homogeneity decreases towards the turbulent regime. In the bubbling/turbulent regime, the bubbles rising through the bed are seen dispersed in the 'continuous phase' or emulsion, indicating that the flow mixture is highly non-homogeneous. Comparative studies were conducted to compare the performance of hydrodynamic models of the FCC regenerator. Lee et al. [32] compared three different models for describing the FCC regenerator, namely the grid effect model, the two-phase model and the bubbling bed model, and compared the simulation results to data from a working refinery FCC unit. They found that the bubbling bed model gave the smallest error in relation to the coke conversion and exit catalyst temperature plant data when the emulsion is considered perfectly mixed for solids, and the dense bed and the freeboard are assumed two thermally uniform stages in series for heat balance. However, they have noted that although the bubbling bed outperformed the two other models, it still was not an exact description of the regenerator. The work of Lee et al. [32] has given results that suggest that the grid effect model is generally more suited for shallow beds (where $\frac{D}{L} \sim 1$) as it was originally developed for such cases [117]. This is in line with the review in Table 4 that shows that only a few researchers have used this model to simulate the regenerator. The more perplexing observation from Table 4, in light of the results from Lee et al. [32], is the limited adoption of the bubbling bed model as opposed to the two-phase model, which was outperformed by the former in terms of both coke conversion and catalyst outlet temperature. One reason for this could be that the two-phase model is much simpler and less computationally expensive. Another reason is that the complexity of the model used is very much linked to the purpose of the model. Models used in the initial design stages are usually shortcut and simple models, whereas control and optimisation models can generally be more involved.

Another issue of note is the treatment of emulsion phase gas mixing or flow. Grace [141] noted that no other feature in fluidised bed reactor modelling has been subject to as many alternative assumptions as the axial mixing of emulsion gas. Table 4 shows that in terms of modelling the FCC regenerator, the behaviour of emulsion phase gas remains unresolved. The assumption for gas in emulsion alternates between well mixed and plug flow in the axial direction. For comparison, Table 4 shows there is some consensus in assuming gas in the bubble phase is plug flow while particles in the emulsion are assumed well mixed. This assumption of plug flow in the bubbles is consistent with the experimental evidence discussed, which suggested that gas starts to deviate from plug flow when solids are introduced to the flow. Because bubbles are assumed to be essentially solid-free, the plug flow of gas is reasonable. However, the emulsion is different because both gas and solids are present in the suspension. While both plug flow and well-mixed assumptions have been used with great utility when describing gas in the emulsion, they are two different flow patterns and therefore mean the understanding of gas mixing in the emulsion as an open question. Levenspiel [142] thoroughly reviewed the problem of emulsion phase gas mixing

in bubbling fluidised beds. They compared results from thirty-nine experiments conducted on group A-type particles by five different reactor groups in various flow reactors, where the extent of conversion was measured during the experiments. They conclude that gas flow in the dense bed cannot be modelled using simple plug flow or well-mixed flow models, and in some cases, these assumptions can be highly inaccurate. Of interest is that parameters can be adjusted in the models so that both sets of assumptions produce results that match measured reactor outlet temperatures, and this is usually sufficient for industrial purposes. The downside is that conditions such as conversion within the dense bed cannot be definitively predicted. Nevertheless, it usually does not affect the exit results which description of emulsion gas is chosen, and until such a time when experiments were conducted to study gas mixing conclusively, this will remain an unsolved aspect of FCC regenerator modelling.

Treatment of bubbles in the bed is also poorly addressed in the regenerator, as can be seen, that many workers of two-phase models have not clearly defined the bubble size or have provided insufficient information for this detail to be discernible to the reader. It may be that this parameter was accounted for in their models but not published in their papers, or it was not treated at all. Workers that properly accounted for bubble size either used a Davidson theory type assumption with uniform bubble size through the bed [128,132,143] or used a correlation for bubble size with height to account for bubble growth through the bed [10,18]. Levenspiel [142] showed that bubble size, for a uniform bubble description in a bubbling bed model, does affect the conversion through the bed. This is consistent with the earlier work [132], which studied the effect of bubble size on oxygen exchange between the emulsion and bubble phase. They reported that smaller bubbles (in the range 5–10 cm) increased the interchange of oxygen between the emulsion and bubble phase resulting in more oxygen being carried to the reacting catalyst surface in the dense bed, while larger bubbles (≥ 20 cm) resulted in lower oxygen interchange and lower coke conversion. Faltsi-Saravelou et al. [132], however, have not addressed the issue of bubble growth through the bed. Nevertheless, a proper description of bubble size needs to be incorporated into dense bed models employing either two-phase or bubbling bed models.

2.4. FCC Regenerator Performance Predictions

Several studies of FCC regenerator modelling have provided simulation results for the axial distribution of gas in the regenerator, the temperature in the bed and the coke conversion. Some of these results are presented in Figure 4 and discussed.

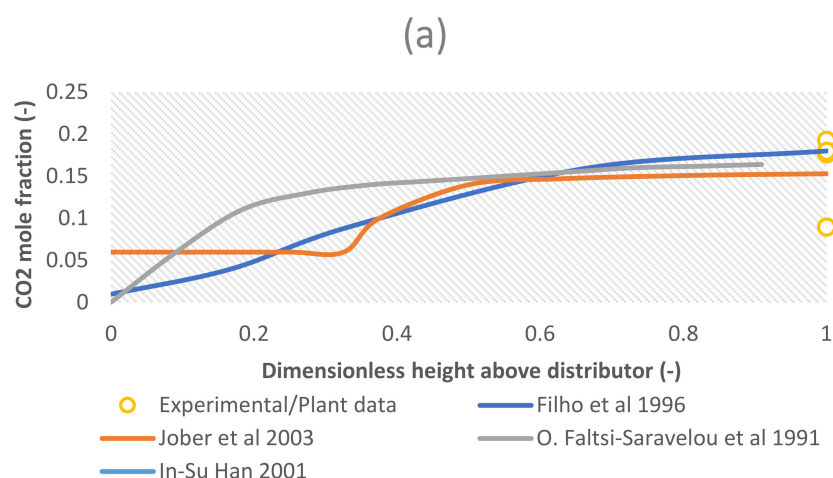


Figure 4. Cont.

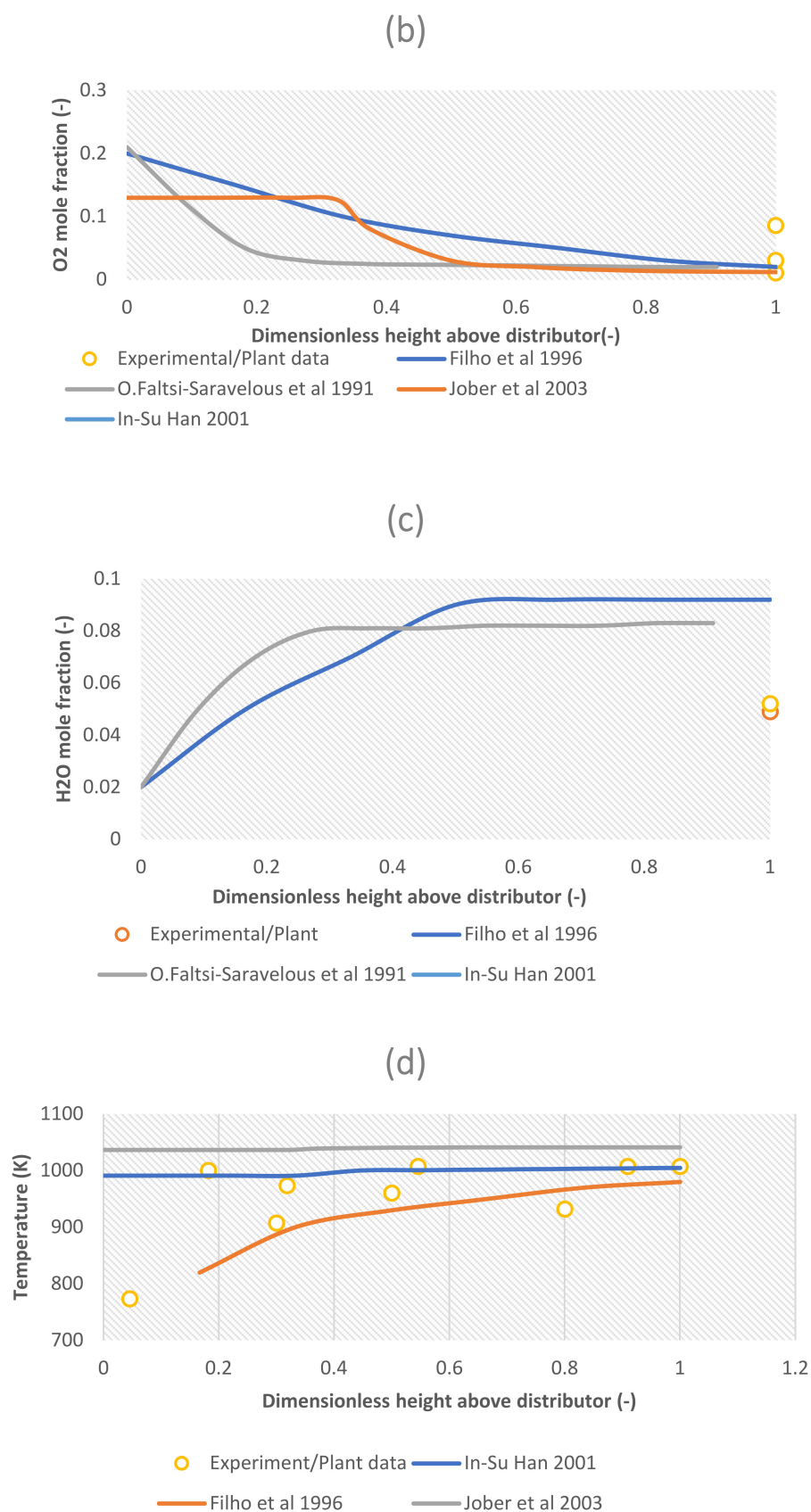


Figure 4. Comparison of predictions from FCC regenerator models in the literature against plant/experimental data for (a) axial profiles of carbon dioxide, (b) axial profiles of oxygen, (c) axial profiles of water vapor and (d) axial profiles of temperature, along the regenerator. Predictions from [18,131,132,134], and plant/experimental data from [19,132,144].

As can be seen, the plant data used here can be divided into two; one where only the exit conditions are reported and the other where conditions along the regenerator are reported (i.e., temperature readings along the regenerator [132]). Figure 4 shows that the exit gas compositions from simulations generally agree well with plant data. However, profiles of gas compositions vary along the riser depending on the flow and mixing pattern assumptions in the dense bed. In Figure 4a,b simulations from Jobber et al. [134] show uniform gas composition in the dense bed while simulations from other workers [18,131,132] show gas profiles increasing for carbon dioxide and decreasing for Oxygen with the height of the dense bed. This is because the former has assumed well-mixed conditions for gases in the dense bed while the latter has assumed plug flow conditions for gases in the dense bed. For data with plug flow gas conditions in dense bed, there is a steep increase (for CO_2 and H_2O) and decrease (for O_2) in the initial stages of the dense bed with the rate decreasing with height. This is because compositions of oxygen from the inlet air are higher in the initial stages of the dense bed, which promotes faster combustions reactions in this region, and as oxygen is used up in air reaching the freeboard, the rates of combustion are lower in this region, and hence only small changes occur in this region. The data and simulations report matching exit flue gas compositions of 15–20 mol% carbon dioxide, 0–5 mol% oxygen and 0–0.2 mol% carbon monoxide. There is a larger discrepancy in plant and simulation results for exit flue gas composition for water vapour. Simulations appear to overestimate the amount of water vapour released from the regenerator. The likely cause of this discrepancy lies in the hydrogen composition in coke (i.e., the moles of hydrogen per mole of carbon in coke). This quantity was proven to depend on the quality and type of gas oil feed used in the riser reactor, meaning some feeds produce coke with higher hydrogen content, therefore corresponding to higher water vapour composition in the regenerator flue gas. The moles of hydrogen per mole of carbon in coke from catalytic cracking of gas oil were reported to vary between 0.4 and 2.0 [32,39]. Simulations of workers [131,132,134] showed that the CO composition leaving the dense bed is higher than zero, but this CO is almost always converted into CO_2 by the time it reaches the regenerator cyclones in the freeboard. This ‘afterburn’ reaction demonstrates the importance of including the freeboard in the FCC regenerator model. de Lasa and Grace [145] also demonstrated that the freeboard is also important because of the influence of the recycling of catalyst particles on coke conversion.

Figure 4d shows the variation in temperature with the height of the regenerator for single regenerator units. Plant data from Faltsi-Saravelou et al. [132] showed that temperature in the regenerator quickly increases in the first 20% of the unit. The initial low temperature is from the mixing of the catalyst with cooler lifting air. The steep increase at the bottom is from combusting reactions releasing exothermic heat that heats up the catalyst and the air flowing through the bed. Higher up the bed increase in temperature is very small because there are reduced reactions in those oxygen lean regions. The temperature in the dense bed is one of the most important variables in the regenerator because heat from the ‘clean’ catalyst is going to be used to provide energy for the endothermic cracking reactions in the riser reactor. Some researchers [19,29,144,146] reported commercial regenerator dense bed temperatures of 907–1040 K. In each case, the difference between dense bed and freeboard temperature is between 3 and 40 K. These data are consistent with simulations results shown in Figure 4d [18,134]. The final temperature in the dense bed is determined by the initial weight fraction of coke on the catalyst, the temperature and flow rate of air through the bed, the catalyst circulation rate and the height of the bed. It is important to note that the temperature description so far has not made a distinction between the temperature of the catalyst and the temperature of the gas; thus far, it was assumed that the temperature is the same. However, as with mass transfer, a resistance in heat transfer between the emulsion and the bubble phase exists, which means that at any height above the distributor plate, the two phases will have different temperatures. Very little data showing this difference have been reported in the literature and in conversion simulation studies, such as those discussed in this paper. Similar to the lack of plant/commercial data

about axial profiles of gas composition in the regenerator, the reason for this is likely linked to the difficulty of making these measurements during the normal operation of the unit. However, regenerator models employing computational fluid dynamics (CFD) tackled this problem correctly [29–31,62,147].

2.5. Shortcomings and Future Recommendations

The following shortcomings were identified from the review of FCC regenerator models:

- (a) Axial mixing: Table 4 shows that the mixing of solids and gas in the bed is usually assumed to be either plug flow or well mixed in the axial direction. Considering the results from Callcott et al. [104] that showed that tracer solids could be completely mixed in the axial direction in 75 s, and also noting that the characteristic residence time for solids in the FCC regenerator is in the range of minutes to an hour (see Table 1), then it is totally reasonable to assume complete mixing for solids in the axial direction. However, gas mixing is more complex, as was explained earlier. It has now been established that the motion of bubbles up the bed causes a rise to circulation patterns of solids in the bed so that solids are moving up the bed in bubbling regions and moving down the bed in regions of low bubbling activity. It was suggested by several workers [16,148] that the regions of downflow of solids drag down the interstitial gas so that downflow of gas is possible in the bed. Stephens et al. [16] suggested that the downflow of gas occurs when the downflow velocity of solids exceeds the velocity of rising emulsion gas. Consequently, this is what has led to back-mixing models for bubbling fluidised beds. The review in Table 4 shows that back-mixing models and their applicability to the FCC regenerator has yet to be explored, and since it has been clear from Levenspiel [142] that plug flow or well-mixed assumptions do not accurately predict gas mixing in the dense bed, it is worth exploring back-mixing models for their performance in describing gas flow in FCC dense beds;
- (b) Radial mixing: According to Grace [141], knowledge of lateral/axial mixing can be far more important than axial mixing in predicting the performance of fluidised units. The FCC regenerator models reviewed in Table 4 are all 1-D models that assume perfect axial mixing of both solids and gases so that any variation that occurs is only in the axial direction. It was described [104] that solids mixing is poor in the lateral (or radial) direction and that complete mixing is only achieved in the time scale in the order of 1.5 h, which exceeds the normal time scale for the residence time of solids in the FCC regenerator (see Table 1). Therefore, it seems unreasonable to assume perfect radial mixing of solids in the regenerator. In order to understand lateral/radial solid mixing better, a lateral dispersion coefficient was used to encompass all the solids mixing processes identified by Rowe and other workers [72,73,149] i.e., emulsion drift, bubble wake lift and bubble eruption scattering. Determination of the dispersion coefficient was generally performed in two ways; (i) a diffusion-type [101,150], where experimental data are fitted to a model that is based on the analogy that solid particles behave similar to gas molecules travelling in a continuous isotropic environment, and (ii) a stochastic-type model [105,151,152] that assumes a solid particle in a bubble induced mixing cell can randomly jump between adjacent mixing cells, and that this jumping is governed by a probability distribution. There has been some success in using these dispersion models, especially in the fields of bubbling fluidised gasification and combustion of coal and biomass, but so far, there is limited literature on their application for FCC regenerator modelling;
- (c) Emissions: in the last three decades, there has been increased scrutiny and regulations on the anthropogenic emissions of GHGs, such as CO , CO_2 , SO_x , CH_4 and NO_x , case in point the Kyoto Protocol of 1997 [7] and the Paris Agreement of 2015 [5]. European countries will report their greenhouse gas emissions reductions as per the approved United Nations Framework Convention on Climate Change (UNFCCC) transparency framework as well as the Intergovernmental Panel on Climate Change (IPCC) methodology guidelines [153]. The reason for such global actions is the

influence of human-made emissions on climate. Fossil Fuel emissions, of which the emissions from the FCC regenerator are a part of, were reported to account for 87% of all the carbon (i.e., CO , CO_2 , CH_4 etc) emissions from anthropogenic sources [154]. Therefore, the ability to predict the emissions of GHGs from the FCC unit is of importance towards the global goals of mitigation of climate change by a reduction in anthropogenic emissions. The current generation of FCC regenerator models (discussed in Table 4) can predict the emissions of carbon-based GHGs because coke burned in the regenerator unit is described as CH_n . However, since other important elements such as nitrogen and sulphur that are precursors to GHGs (NO_x and SO_x , respectively) and are present in coke but have been ignored in modelling, which means the current models are unable to predict these emissions. Hence, considering the gravity of the climate change problem, it is recommended that future models include kinetics for the combustion of sulphur and nitrogen so that their emission gases can be monitored and addressed;

- (d) Temperature: A common assumption in modelling is to assume that there is thermodynamic equilibrium between the gas and the solids in the emulsion phase. This treats any resistance to heat transfer at the solid–gas interphase as negligible. Since the temperature of the catalyst is an important parameter in the FCC regenerator, the rate of heat transfer between the catalyst particle and the gas plays an important role in the performance of the unit since it determines the energy balance. For design purposes, this assumption is usually sufficient [155]. However, since the heat capacity and thermal conductivity values for the catalyst are usually appreciably higher than that of the gas, for cases where a more detailed description of the temperature of gas and catalyst is required, arguably in the case of the FCC regenerator for its influence on riser thermal balance, the loosening of the thermal equilibrium assumption may be worth exploring;
- (e) Bubble properties: from examining Table 4, it is easy to see that the bubbles rising through the dense bed of the FCC regenerator have generally been poorly described in the models. Bubbles affect the gas–solid contact in the bed and therefore control mass and heat transfer in the bed; hence, their modelling in two-phase or bubbling beds is of great importance to the prediction of coke conversion and thermal balance in the regenerator. Although the understanding of bubble size, growth and frequency is highly empirical, these empirical correlations provide a great understanding of the bubbling phenomena in the dense bed and should be included in the modelling of the FCC regenerator.

3. Modelling FCC Unit Constitutive Components

3.1. Cyclones

Cyclones are usually used in both the reactor and the regenerator systems of an FCC unit. They are the conventional industry equipment used to separate gas–solid two-phase flow. In the FCC reactor system, the cyclones are used in the disengaging section to separate entrained catalyst particles from the wet gases going to the main fractionating column. In the FCC regenerator, the cyclones are used to separate any entrained catalyst particles escaping at the top of the freeboard from the flue gases leaving the regenerator system. The most used type of cyclone in these systems is the tangential inlet cyclone that uses turbulent swirling flow to separate the high-density entrained phase (the catalyst particulate phase) from the low-density carrier phase (the gas) [156]. The swirling flow pattern usually consists of a double vortex flow pattern; an outer vortex with downward axial velocity and an inner vortex with upward axial velocity, shown in Figure 5a. The outer vortex loses its downward momentum towards the bottom of the cyclone and subsequently changes direction to flow upwards, resulting in the inner vortex being formed [156]. Because of the complex nature of the flow inside the cyclone, this flow pattern influences some of the important operational parameters, such as the separation efficiency and the pressure drop [156]. For this reason, these parameters are usually estimated using CFD, where

the anisotropic turbulence and localised flow field at short time and space scales can be considered [157]. However, because CFD is beyond the scope of the current work, only the global balances over the cyclone are carried out to model the system.

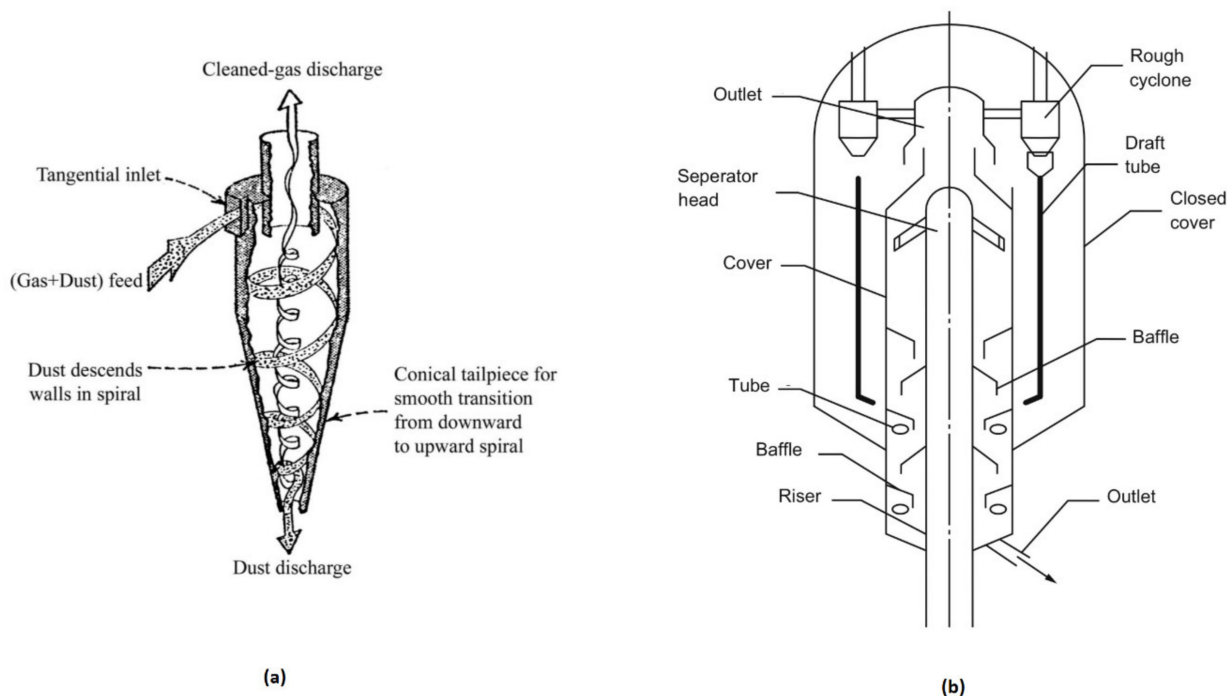


Figure 5. (a) vortex flow patterns inside a tangential inlet cyclone [158], (b) a basic vortex quick separation showing a multi-cyclone system for FCC reactor termination [159].

Similar to the disengaging–stripping section, the cyclone model consists of balances for mass and energy and estimation of pressure drop. Pressure drop and separation efficiency are the most important performance parameters for the operation of a cyclone [156,157,160–163]. Before balances can be made, the current approach requires that efficiency and pressure drop be quantities that are known (specified) or be quantities that can be predicted based on the operating conditions. Experimental data from the literature have shown that these performance indicators are dependent on solid loading, gas and solid flow rates, gas and solid properties (such as particle size, gas viscosity, etc.), temperature and entry effects, and cyclone geometry [157,160,162,164–166]. Traditionally, prediction of the performance indicators is such that a function of the above-mentioned variables is developed to predict the indicator. Several methods for estimating efficiency are well established in the literature: time-of-flight correlation, the equilibrium orbit model and the fractional efficiency method [167–171]. Zhang and Basu [163] developed the following semi-empirical correlation (Equation (16)) for the collection efficiency of gas–solid cyclones using equilibrium orbit theory:

$$\eta = 1 - \exp\left(-\frac{1.04\delta^{3.9}}{0.002Re_0^5 - 0.0102Re_0^3\delta^{1.3} + 0.416Re_0^{0.58}\delta^{3.15}}\right) \quad (16)$$

with Re as the Reynolds number based on particle diameter and subscript 0 denotes that Re is taken at the bottom of the cyclone where the conical radius is r_0 . Traditionally, correlations for η are made such that $\eta = f(Re, St)$ where St is the well-known Stokes number. However, Zhang and Basu [163] chose their correlation such that $\eta = f(Re, \delta)$ as they noted that this correlated better compared to the traditional Reynolds–Stokes approach. In this case, δ (in Equation (17)) is the non-dimensional ratio of the radius of the particle

orbit in the cyclone to the radius at the exit (i.e., $\frac{r}{r_0}$). Without much loss of accuracy, the workers [163] found that:

$$\delta = \left(\frac{2\pi St}{B^2} \right)^{\frac{1}{2\alpha}} \quad (17)$$

For:

$$B = \frac{\frac{1}{1-\alpha} \left(\left(\frac{R}{r_0} \right)^{1-\alpha} - 1 \right)}{\frac{R}{r_0} - 1} \quad (18)$$

where α is an exponent of the velocity distribution of the free vortex and can be obtained empirically from different sizes of cyclones. Zhang and Basu found a value of $\alpha = -0.65$. Thus, from the above analysis, for known process and stream conditions of the cyclone, the collection efficiency can be predicted. In both the reactor and the regenerator systems, the entrained catalyst is separated from the gas phase using a multi-stage cyclone system rather than just a single cyclone to maximise the separation and the throughput. In order to carry out the conservation balance equations, it is usually assumed that all cyclones are identical (both in terms of dimensions and flow conditions) for simplicity, the flow rate through the cyclone dipleg is controlled by the holdup in the cyclone, no reactions occur in the cyclone because the flows are considered dilute with small solid loadings and cyclones are in thermal equilibrium with the disengaging section since this is where they are located [10]. Therefore, only material balances are required in this case for modelling the cyclone systems. The temperature of flow into and out of the cyclones is therefore constant and is determined by energy balances in the disengaging section. The thermal equilibrium assumption is valid because no reactions are assumed to occur in the cyclone, no new streams are present, and at a steady state, the cyclone body approaches the surrounding (disengaging section) temperature; hence, it is reasonable to assume that temperature does not change in the cyclone. Considering the mentioned assumptions, Han and Chung [10] showed that for a reactor system with N_{CY} cyclones, the pseudo-steady state catalyst balance for the cyclones under continuous stirred tank assumption is given by Equation (19):

$$w_{cCY} = \frac{\rho_b N_{CY}}{A_{CYd}} \left(\frac{\eta_{CY} v_{cCY} w_{cST} A_{CYi}}{k_{vCY} V_{ST}} \right)^2 \quad (19)$$

where A_{CY} is the area of the cyclone at the inlet (i) and at the dipleg (d), and v_{cCY} is the velocity at the inlet of the cyclone, which may be calculated using the Rosin, Rammler and Intelmann equation in Equation (20) [172]:

$$v_{cCY} = \frac{9\mu_g A_{CYi}}{d_{cm} \pi N_{CYt} \left(\rho_c - \frac{w_{gST}}{V_{gST}} \right) h_{CYi}} \quad (20)$$

where d_{cm} is the minimum particle diameter completely separated by the cyclone system, and N_{CYt} is the number of 360° turns made spirally down the cyclone. For typical industrial cyclones, N_{CYt} ranges from 1 to 10 and can be estimated from the cyclone geometry by Equation (21) [173]:

$$N_{CYt} = \frac{1}{H} \left(\frac{L_b + \left(\frac{L_c}{2} \right)}{H} \right) \quad (21)$$

where H is the height of the cyclone inlet mouth, and L_b and L_c are heights of the cyclone body and conical base, respectively. Since the holdup, inlet velocity of the catalyst and the cyclone separation efficiency are known, the flow rate of catalyst entrained with gas that is not captured by the cyclone, F_{cMF} , that flows to the main fractionating unit and the

flow rate gas from the cyclone to the main fractionating unit, F_{gMF} , can be determined by Equations (22) and (23), respectively [10]:

$$F_{cMF} = (1 - \eta_{CY})v_{cCY}A_{CYi} \left(\frac{w_{cCY}}{V_{ST}} \right) N_{CY} \quad (22)$$

$$F_{gMF} = K_{vMF} \sqrt{P_{ST} - P_{MF}} \quad (23)$$

Note that for flow rates in the regenerator cyclones, the above equations would calculate the flow rate of catalyst and gas that make up the flue gas stack. Flow rates through the dipleg can be calculated via simple balances between inlet flow rates into the cyclone and the flow rates leaving at the top of the cyclone for steady state operation. As previously stated, a pressure drop is also an important performance indicator for cyclone operation. Pressure loss in a cyclone is usually divided according to different contributions [174,175]: head losses at the cyclone inlet, losses in the separation space due to gas flow and the wall and losses in the vortex finder mainly due to gas reversal and contraction at the exit. The relative magnitudes of the losses depend on the cyclone classification as either low-loaded or high-loaded [171,176]. It was already established that solid loading for the FCC cyclones might be assumed to be small; therefore, it can be assumed to be low-loaded. For low-loaded conditions, Chen and Shi [175] and Li et al. [177] showed that the contributions of outlet pressure losses might be ignored. Chen and Shi [175] developed a 'universal' method that predicts the pressure losses of a cyclone, the so-called C-S method, and this method is now widely used in the literature and was subsequently improved for better accuracy by Li et al. [177], especially for high-loaded cases. The C-S model predicts that from Equation (24):

$$\Delta P_{CY} = \frac{1}{2} \rho_g \xi_{CY} U_g \quad (24)$$

where U_g is either the inlet or the outlet gas velocity and ξ_{CY} is the dimensionless pressure drop parameter. In the literature, two main methods of determining ξ are usually used [171]: the first method accounts for effects of cyclone geometry and solid loading on pressure losses (e.g., $\xi_{CY} = \xi_{\text{geometry}} \times \xi_{\text{solid}}$) [178], and the second method sums the individual contributions to pressure loss (e.g., $\xi_{CY} = \xi_{\text{in}} + \xi_{\text{body}} + \xi_{\text{vortex}} + \xi_{\text{out}}$) [170,175]. Chen and Shi [175] proposed Equation (25) for ξ_{CY} for dust-laden flows:

$$\xi_{CY} = \left(1 + \frac{C_i}{\rho_g}\right) \left(1 - \left(\frac{2k_i \tilde{b}}{1 + 1.33\tilde{b} - \tilde{d}_r}\right)^2 + 1.11fK_A \tilde{F}_s \tilde{V}_{\theta w} \tilde{d}_r^{-1.5n} + \frac{\tilde{V}_{\theta w}^2}{\left(\tilde{r}_c \tilde{d}_r\right)^n} + \frac{1}{K_A^2 \left(\tilde{d}_r^2 - \tilde{r}_c^2\right)^2}\right) \quad (25)$$

where the (\sim) indicates a nondimensional variable. C_i is the inlet solid loading (kg of inlet solid/m³ of inlet gas), k_i is a correction coefficient of expansion loss (≈ 0.3) [162], f is the friction coefficient (≈ 0.005 for steel cyclones) [162] and K_A is the inlet area ratio ($= \frac{\pi D^2}{4ab}$; for D cyclone barrel diameter and a, b for cyclone inlet width and height). Non-dimensional variables are such that \tilde{b} is dimensional width ($= \frac{b}{D}$), \tilde{F}_s dimensionless contact area, \tilde{r}_c is the dimensionless radius of core flow ($= \frac{r_c}{R}$), \tilde{d}_r is the dimensionless cyclone outlet diameter ($= \frac{d_r}{D}$) and $\tilde{V}_{\theta w}$ is the dimensionless tangential velocity at radius R ($= \frac{V_{\theta w}}{U_g}$). Chen and Shi [175] correlated \tilde{r}_c with \tilde{d}_r in Equation (26):

$$\tilde{r}_c = 0.38\tilde{d}_r + 0.5\tilde{d}_r^2 \quad (26)$$

Additionally, the dimensionless tangential velocity at the cyclone wall is given by Equation (27) [162]:

$$\tilde{V}_{\theta w} = \frac{1.11K_A^{-0.21}\tilde{d}_r^{0.16} Re^{0.06}}{1 + f\tilde{F}_s\sqrt{K_A\tilde{d}_r}} \quad (27)$$

For

$$Re = \frac{\rho_g U_g D}{\mu_g K_A \tilde{d}_r} \quad (28)$$

Note that different workers in the literature and no doubt in the industry have developed alternative equations for ξ_{CY} and $\tilde{V}_{\theta w}$. Therefore, the choice of expression must be based on their ranges of applicability, especially in terms of solid loading, which has a great impact on the pressure drop of a cyclone.

3.2. Catalyst Transport Lines

The transport lines carry catalysts between the reactor and the regenerator systems. The catalyst circulation rate within the transport lines is controlled by a slide valve that should be attached to the line [10,18]. In terms of the dynamics of both units, the circulation rate with the transport lines affects the holdup of catalyst in the regenerator and the disengaging–stripper section of the reactor; hence, it affects the coupling of the two systems. This coupling makes the catalyst transport line and associated valves important features for any model of the FCC unit. By taking the pressure across the slide valve into account, the flow rate of catalyst through the transport line can be calculated from Equation (29) [10,18]:

$$F_{cV} = k_v f_v(x_v) \sqrt{\Delta P} \quad (29)$$

where F_{cV} is the catalyst flow rate through the valve, k_v is the valve flow rating factor and $f_v(x_v)$ is the valve flow characteristic function. ΔP is the pressure drop across the valve, which depends on the direction of catalyst flow; for example, for the spent catalyst transport line, the ΔP is the pressure difference between the bottom of the stripper and the regenerator dense bed. In this example, F_{cV} is catalyst flow rate out of the stripper and the catalyst flow rate into the dense bed. Because the catalyst residence time inside the transport lines is in the order of a few seconds, its influence on the regenerator, and therefore the whole FCC unit, is small so that the transport lag may be ignored [10,135]. This assumption therefore leads to negligible energy loss through the transport line so that catalyst retains the temperature of the vessel it is leaving so that no further energy balance is required. However, some workers have explicitly described the valve characteristics in their model but instead provided catalyst circulation rate as a specification based on plant data [19]. In such cases, models are unsuitable to use to study the effects of changes in flow conditions on the unit dynamics because the coupling of the pressure drop across the vessels and valve characteristics with the rest of the unit has been removed, which could lead to inaccurate predictions. Nevertheless, such studies presented useful results in terms of conversions in both reactor systems.

4. Conclusions

Overall, modelling of the FCC unit using traditional reaction engineering approaches has certainly come a long way. The kinetics of the regenerator is now well understood, with models published able to predict the emissions of carbon monoxide and carbon dioxide that are produced during the combustion reactions. Additionally, analytical technology had come a long way since the early 1960s when FCC modelling first began, with tools now able to characterise coke at the elemental level. This means researchers are now able to incorporate elements such as sulphur and nitrogen into their kinetic models to predict greenhouse gas emissions such as SO_x and NO_x that are also directly produced during the combustion reactions in the regenerator. Due to the current global action against climate,

we recommend that future models make necessary changes to incorporate the combustion of sulphur and nitrogenous compounds, which are also present in the coke. In terms of hydrodynamics, both the fluidised bed reactor vessels of the FCC unit have significant flow heterogeneity during their normal operation. In the regenerator, the heterogeneity arises from bubbles rising through the emulsion, whereas in the riser clusters of catalyst particles are observed in the suspension. This heterogeneity is important to the conversion in both vessels and has been modelled to varying degrees by researchers. More recently, the study of such flow patterns is being conducted via CFD, providing detail that is seldom captured experimentally or via traditional modelling simulations.

Author Contributions: Conceptualization, T.W.S., R.P., I.M.M. and Y.M.J.; methodology, T.W.S. and Y.M.J.; software, T.W.S.; validation, T.W.S. and Y.M.J.; formal analysis, T.W.S., R.P., I.M.M., Y.M.J.; investigation, T.W.S. and Y.M.J.; resources, T.W.S., R.P., I.M.M., Y.M.J.; data curation, T.W.S.; writing—original draft preparation, T.W.S.; writing—review and editing, T.W.S., R.P., I.M.M., Y.M.J.; visualization, T.W.S.; supervision, R.P., I.M.M., Y.M.J. All authors have read and agreed to the published version of the manuscript.

Funding: This research received no external funding.

Institutional Review Board Statement: Not applicable.

Informed Consent Statement: Not applicable.

Acknowledgments: The main author (T.W.S.) would like to acknowledge the Government of Botswana for funding his Ph.D. research studies.

Conflicts of Interest: There is no conflict of interest regarding the publication of this research.

Nomenclature

Symbol	Description	Units
C	Molar concentration	kmol m^{-3}
D	Dispersion coefficient	$\text{m}^2 \cdot \text{s}^{-1}$
d_p	Particle diameter	m
d_{cm}	Smallest particle diameter separated by cyclone	m
F	Mass flow rate	$\text{kg} \cdot \text{s}^{-1}$
g	Acceleration due to gravity	ms^{-2}
h	Height of jet penetration through the bed	$\text{mkJ} \cdot \text{kg}^{-1}$
	Enthalpy of the phase	
k	Deviation coefficient from ideal two-phase flow	(-)/varied
	Reaction rate constant	
K	Interphase mass transfer coefficient	ms^{-1}
n	Reaction order	(-)(-)
	Molar ratio of hydrogen to Carbon in coke	
N	Molar flux	$\text{kmol} \cdot \text{m}^{-2} \cdot \text{s}^{-1}$ (-)
	Number of cyclones	
N_{CYt}	Number of 360° turns made spirally down a cyclone	(-)
P	Pressure	kPa
r	Reaction rate	$\text{kmol m}^{-3} \cdot \text{s}^{-1} \cdot \text{kPa} \cdot \text{s}^{-1}$
R	Component reaction rate	$\text{kmol} \cdot \text{m}^{-3} \cdot \text{s}^{-1} \cdot \text{kJ} \cdot \text{kmol}^{-1} \cdot \text{K}^{-1}$
	Ideal gas constant	
Re	Reynolds number	(-)
S	Energy source term	$\text{kJ} \cdot \text{s}^{-1}$
T	Temperature	K
U_b	Bubble rise velocity	$\text{m} \cdot \text{s}^{-1}$
U_c	Gas circulation velocity inside rising bubbles	$\text{m} \cdot \text{s}^{-1}$
U_{mb}	Minimum bubbling velocity	$\text{m} \cdot \text{s}^{-1}$
U_{mf}	Minimum fluidisation velocity	$\text{m} \cdot \text{s}^{-1}$
U_t	Terminal velocity of particles in the bed	$\text{m} \cdot \text{s}^{-1}$
V	Volume	m^3

w	Mass of holdup in reactor or cyclone	kg
x	Mole fraction	(–)
Y	Deviation coefficient from ideal two-phase flow	(–)
Greek letters and other symbols		
ε	Volume fraction	(–)
α	Exponent of velocity distribution in a cyclone vortex	(–)
β	Molar ratio of CO to CO ₂	(–)
ρ	Density	kg.m ^{−3}
δ	Ratio of particle radius to radius of the cyclone	(–)
η	Cyclone separation efficiency	(–)
ξ	Cyclone Pressure drop parameter	(–)
$\tilde{V}_{\theta w}$	Dimensionless tangential velocity at cyclone wall	(–)
ΔQ	Heat of reaction	kJ.s ^{−1}
ΔP	Pressure drop	kPa
ΔH	Enthalpy change of reaction	kJ.kmol ^{−1}
Subscripts		
e	Emulsion	
b	Bubble phase	
be	Bubble to emulsion	
eb	Emulsion to bubble	
CO	Carbon monoxide	
C	Coke	
CO ₂	Carbon dioxide	
H ₂ O	Water vapor	
c	Catalyst	
g	Gas	

References

- Arbel, A.; Huang, Z.; Rinard, I.H.; Shinnar, R.; Sapre, A.V. Dynamic and Control of Fluidized Catalytic Crackers. 1. Modeling of the Current Generation of FCC's. *Ind. Eng. Chem. Res.* **1995**, *34*, 1228–1243. [[CrossRef](#)]
- Sadeghbeigi, R. *Fluid Catalytic Cracking Handbook: An Expert Guide to the Practical Operation, Design, and Optimization of FCC Units*; Butterworth-Heinemann: Oxford, UK, 2012. [[CrossRef](#)]
- Kim, S.W.; Kim, S.D. Void properties in dense bed of cold-flow fluid catalytic cracking regenerator. *Processes* **2018**, *6*, 80. [[CrossRef](#)]
- Wetherald, R.T.; Manabe, S. Sensitivity Studies of Climate Involving Changes in CO₂ Concentration. *Dev. Atmos. Sci.* **1979**, *10*, 57–64. [[CrossRef](#)]
- UNFCCC. Paris Agreement. *Int. Leg. Mater.* **2016**, *55*, 740–755. [[CrossRef](#)]
- UNFCCC. National Inventory Submissions 2020 | UNFCCC n.d. Available online: <https://unfccc.int/ghg-inventories-annex-i-parties/2020> (accessed on 28 June 2021).
- UNFCCC. Kyoto Protocol to the United Nations Framework Convention on Climate Change. *Am. J. Int. Law* **1998**, *92*, 315–331. [[CrossRef](#)]
- Berruti, F.; Pugsley, T.S.; Godfroy, L.; Chaouki, J.; Patience, G.S. Hydrodynamics of circulating fluidized bed risers: A review. *Can. J. Chem. Eng.* **1995**, *73*, 579–602. [[CrossRef](#)]
- Grace, J.R.; Avidan, A.A.; Knowlton, T.M. *Circulating Fluidized Beds*; Blackie Academic & Professional: London, UK, 1997.
- Han, I.S.; Chung, C.B. Dynamic modeling and simulation of a fluidized catalytic cracking process. Part I: Process modeling. *Chem. Eng. Sci.* **2001**, *56*, 1951–1971. [[CrossRef](#)]
- Kunii, D.; Levenspiel, O. *Fluidization Engineering*; Butterworth-Heinemann: Oxford, UK, 1991.
- Shah, M.; Utikar, R.; Pareek, V.; Evans, G.; Joshi, J. Computational fluid dynamic modelling of FCC riser: A review. *Chem. Eng. Res. Des.* **2016**, *1*, 403–448. [[CrossRef](#)]
- Toomey, R.D.; Johnstone, H.F. Gas Fluidization of Solid Particles. *Chem. Eng. Prog. Vol.* **1952**, *48*, 220–226.
- Kunii, D.; Levenspiel, O. *Fluidization Engineering*; John Wiley and Sons: New York, NY, USA, 1969.
- Kunii, D.; Levenspiel, O. Bubbling bed model: Model for the Flow of Gas through a Fluidized Bed. *Ind. Eng. Chem. Fundam.* **1968**, *7*, 446–452. [[CrossRef](#)]
- Stephens, G.K.; Sinclair, R.J.; Potter, O.E. Gas exchange between bubbles and dense phase in a fluidised bed. *Powder Technol.* **1967**, *1*, 157–166. [[CrossRef](#)]
- Kato, K.; Wen, C.Y. Bubble assemblage model for fluidized bed catalytic reactors. *Chem. Eng. Sci.* **1969**, *24*, 1351–1369. [[CrossRef](#)]
- Han, I.S.; Chung, C.B. Dynamic modeling and simulation of a fluidized catalytic cracking process. Part II: Property estimation and simulation. *Chem. Eng. Sci.* **2001**, *56*, 1973–1990. [[CrossRef](#)]

19. Ali, H.; Rohani, S.; Corriou, J.P. Modelling and control of a riser type fluid catalytic cracking (FCC) unit. *Chem. Eng. Res. Des.* **1997**, *75*, 401–412. [[CrossRef](#)]
20. Yakubu, J.M.; Patel, R.; Mujtaba, I.M. Optimization of fluidized catalytic cracking unit regenerator to minimize CO₂ emissions. *Chem. Eng. Trans.* **2017**, *57*, 1531–1536. [[CrossRef](#)]
21. Arthur, J.R. Reactions between Carbon and Oxygen. *Trans. Faraday Soc.* **1951**, *47*, 164–178. [[CrossRef](#)]
22. Weisz, P.B. Corn bustion of Carbonaceous Deposits within Porous Catalyst Particles III. The CO₂/CO Product Ratio. *J. Catal.* **1966**, *6*, 425–430. [[CrossRef](#)]
23. Weisz, P.B.; Goodwin, R.B. Combustion of Carbonaceous Deposits within Porous Catalyst Particles II. Intrinsic Burning Rate. *J. Catal.* **1966**, *6*, 227–236. [[CrossRef](#)]
24. Weisz, P.B.; Goodwin, I.D. Combustion of Carbonaceous Deposits within Porous Catalyst Particles I. Diffusion-Controlled Kinetics. *J. Catal.* **1963**, *2*, 397–404. [[CrossRef](#)]
25. Tone, S.; Miura, S.-I.; Otake, T. Kinetics of Oxidation of Coke on Silica-Alumina Catalysts. *Bull. Jpn. Pet. Inst.* **1972**, *14*, 76–82. [[CrossRef](#)]
26. Hano, T.; Nakashio, F.; Kusunoki, K. The burning rate of coke deposited on zeolite catalyst. *J. Chem. Eng. Jpn.* **1975**, *8*, 127–130. [[CrossRef](#)]
27. Wang, G.X.; Lin, S.X.; Mo, W.J.; Peng, C.L.; Yang, G.H. Kinetics of Combustion of Carbon and Hydrogen in Carbonaceous Deposits on Zeolite-Type Cracking Catalysts. *Ind. Eng. Chem. Process Des. Dev.* **1986**, *25*, 626–630. [[CrossRef](#)]
28. Arandes, J.M.; Abajo, I.; Fernández, I.; López, D.; Bilbao, J. Kinetics of gaseous product formation in the coke combustion of a fluidized catalytic cracking catalyst. *Ind. Eng. Chem. Res.* **1999**, *38*, 3255–3260. [[CrossRef](#)]
29. Amblard, B.; Singh, R.; Gbordzoe, E.; Raynal, L. CFD modeling of the coke combustion in an industrial FCC regenerator. *Chem. Eng. Sci.* **2017**, *170*, 731–742. [[CrossRef](#)]
30. Hosseini, S.H.; Rahimi, R.; Zivdar, M.; Samimi, A. CFD simulation of gas-solid bubbling fluidized bed containing FCC particles. *Korean J. Chem. Eng.* **2009**, *26*, 1405–1413. [[CrossRef](#)]
31. Azarnivand, A.; Behjat, Y.; Safekordi, A.A. CFD simulation of gas-solid flow patterns in a downscaled combustor-style FCC regenerator. *Particuology* **2018**, *39*, 96–108. [[CrossRef](#)]
32. Lee, L.S.; Yu, S.W.; Cheng, C.T.; Pan, W.Y. Fluidized-bed catalyst cracking regenerator modelling and analysis. *Chem. Eng. J.* **1989**, *40*, 71–82. [[CrossRef](#)]
33. Qian, K.; Tomczak, D.C.; Rakiewicz, E.F.; Harding, R.H.; Yaluris, G.; Cheng, W.C.; Zhao, X.; Peters, A.W. Coke formation in the fluid catalytic cracking process by combined analytical techniques. *Energy Fuels* **1997**, *11*, 596–600. [[CrossRef](#)]
34. Luan, H.; Lin, J.; Xiu, G.; Ju, F.; Ling, H. Study on compositions of FCC flue gas and pollutant precursors from FCC catalysts. *Chemosphere* **2020**, *245*, 125528. [[CrossRef](#)]
35. Ibarra, Á.; Veloso, A.; Bilbao, J.; Arandes, J.M.; Castaño, P. Dual coke deactivation pathways during the catalytic cracking of raw bio-oil and vacuum gasoil in FCC conditions. *Appl. Catal. B Environ.* **2016**, *182*, 336–346. [[CrossRef](#)]
36. Elshishini, S.S.; Elnashaie, S.S.E.H. Digital simulation of industrial fluid catalytic cracking units: Bifurcation and its implications. *Chem. Eng. Sci.* **1990**, *45*, 553–559. [[CrossRef](#)]
37. Bai, D.; Zhu, J.X.; Jin, Y.; Yu, Z. Simulation of FCC catalyst regeneration in a riser regenerator. *Chem. Eng. J.* **1998**, *71*, 97–109. [[CrossRef](#)]
38. Bayraktar, O.; Kugler, E.L. Coke content of spent commercial fluid catalytic cracking (FCC) catalysts: Determination by temperature-programmed oxidation. *J. Therm. Anal. Calorim.* **2003**, *71*, 867–874. [[CrossRef](#)]
39. Hashimoto, K.; Takatani, K.; Iwasa, H.; Masuda, T. A multiple-reaction model for burning regeneration of coked catalysts. *Chem. Eng. J.* **1983**, *27*, 177–186. [[CrossRef](#)]
40. Dimitriadis, V.D.; Lappas, A.A.; Vasalos, I.A. Kinetics of combustion of carbon in carbonaceous deposits on zeolite catalysts for fluid catalytic cracking units (FCCU). Comparison between Pt and non Pt-containing catalysts. *Fuel* **1998**, *77*, 1377–1383. [[CrossRef](#)]
41. Morley, K.; De, L. On the Determination of Regeneration of Kinetic Parameters for the Cracking Catalyst. *Can. J. Chem. Eng.* **1987**, *65*, 773–777. [[CrossRef](#)]
42. Howard, J.B.; Williams, G.C.; Fine, D.H. Kinetics of Carbon Monoxide Oxidation in Postflame Gases. In *Symposium (International) on Combustion*; Elsevier: Amsterdam, The Netherlands, 1973.
43. Li, C.; Brown, T.C. Carbon oxidation kinetics from evolved carbon oxide analysis during temperature-programmed oxidation. *Carbon* **2001**, *39*, 725–732. [[CrossRef](#)]
44. Kanervo, J.M.; Krause, A.O.I.; Aittamaa, J.R.; Hagelberg, P.H.; Lipiäinen, K.J.T.; Eilos, I.H.; Hiltunen, J.S.; Niemi, V.M. Kinetics of the regeneration of a cracking catalyst derived from TPO measurements. *Chem. Eng. Sci.* **2001**, *56*, 1221–1227. [[CrossRef](#)]
45. Williams, G.C.; Hottel, H.C.; Morgan, A.C. The Combustion of Methane in a Jet-Mixed Reactor. In *Symposium (International) on Combustion*; Elsevier: Amsterdam, The Netherlands, 1969; Volume 12, pp. 913–925. [[CrossRef](#)]
46. Schneider, G.R. Kinetics of Propane Combustion in a Well Stirred Reactor. Ph.D. Thesis, Massachusetts Institute of Technology, Department of Nuclear Engineering, Cambridge, MA, USA, 1961.
47. Friedman, R.; Cyphers, J.A. Flame structure studies. III. Gas sampling in a low-pressure propane-air flame. *J. Chem. Phys.* **1955**, *23*, 1875–1880. [[CrossRef](#)]

48. Singh, T.; Sawyer, R.F. CO Reactions in the Afterflame Region of Ethylene/Oxygen and Ethane/Oxygen Flames. In *Symposium (International) on Combustion*; Elsevier: Amsterdam, The Netherlands, 1971; Volume 13, pp. 403–416. [\[CrossRef\]](#)
49. Sobolev, G.K. High-Temperature Oxidation and Burning of Carbon Monoxide. In *Symposium (International) on Combustion*; Elsevier: Amsterdam, The Netherlands, 1958; Volume 7, pp. 386–391. [\[CrossRef\]](#)
50. Ghazal, F.P.H. Kinetics of Carbon Monoxide Oxidation in Combustion Products. Ph.D. Thesis, Massachusetts Institute of Technology, Cambridge, MA, USA, 1971.
51. Morley, K.; de Lasa, H.I. Regeneration of cracking catalyst influence of the homogeneous CO postcombustion reaction. *Can. J. Chem. Eng.* **1988**, *66*, 428–432. [\[CrossRef\]](#)
52. Ahmed, S.; Back, M.H. The role of the surface complex in the kinetics of the reaction of oxygen with carbon. *Carbon* **1985**, *23*, 513–524. [\[CrossRef\]](#)
53. Tucker, B.G.; Mulcahy, M.F.R. Formation and decomposition of surface oxide in carbon combustion. *Trans. Faraday Soc.* **1969**, *65*, 274–286. [\[CrossRef\]](#)
54. Geldart, D. Types of gas fluidization. *Powder Technol.* **1973**, *7*, 285–292. [\[CrossRef\]](#)
55. Baeyens, J.; Geldart, D. Predictive Calculations of Flow Parameters in Gas Fluidized Beds and Fluidization Behaviour of Various Powders. In *Proceedings the International Symposium Fluidization and Its Applications*; Cepadues Edition: Toulouse, France, 1973; p. 263.
56. Yates, J.G. *Fundamentals of Fluidized-Bed Chemical Processes: Butterworths Monographs in Chemical Engineering*; Butterworth-Heinemann: Oxford, UK, 1983.
57. Kumar, A.; sen Gupta, P. Prediction of minimum fluidization velocity for multicomponent mixtures. *Indian J. Technol.* **1974**, *12*, 225–227.
58. Mawatari, Y.; Tatemoto, Y.; Noda, K. Prediction of minimum fluidization velocity for vibrated fluidized bed. *Powder Technol.* **2003**, *131*, 66–70. [\[CrossRef\]](#)
59. Rowe, P.N.; Nienow, A.W. Minimum fluidisation velocity of multi-component particle mixtures. *Chem. Eng. Sci.* **1975**, *30*, 1365–1369. [\[CrossRef\]](#)
60. Asif, M. Predicting minimum fluidization velocities of multi-component solid mixtures. *Particuology* **2013**, *11*, 309–316. [\[CrossRef\]](#)
61. Delebarre, A. Revisiting the Wen and Yu equations for minimum fluidization velocity prediction. *Chem. Eng. Res. Des.* **2004**, *82*, 587–590. [\[CrossRef\]](#)
62. Amarasinghe, W.S.; Jayarathna, C.K.; Ahangama, B.S.; Tokheim, L.A.; Moldestad, B.M.E. Experimental Study and CFD Modelling of Minimum Fluidization Velocity for Geldart A, B and D Particles. *Int. J. Model. Optim.* **2017**, *7*, 152–156. [\[CrossRef\]](#)
63. Zhang, X.; Zhou, Y.; Zhu, J. Enhanced fluidization of group A particles modulated by group C powder. *Powder Technol.* **2021**, *377*, 684–692. [\[CrossRef\]](#)
64. Lee, J.R.; Lee, K.S.; Hasolli, N.; Park, Y.O.; Lee, K.Y.; Kim, Y.H. Fluidization and mixing behaviors of Geldart groups A, B and C particles assisted by vertical vibration in fluidized bed. *Chem. Eng. Process. Process Intensif.* **2020**, *149*, 107856. [\[CrossRef\]](#)
65. Frank, D.J.; Roland, C.; David, H. *Fluidization*, 2nd ed.; Academic Press Inc.: Cambridge, MA, USA, 1985.
66. Anantharaman, A.; Cocco, R.A.; Chew, J.W. Evaluation of correlations for minimum fluidization velocity (Umf) in gas-solid fluidization. *Powder Technol.* **2018**, *323*, 454–485. [\[CrossRef\]](#)
67. Shaul, S.; Rabinovich, E.; Kalman, H. Generalized flow regime diagram of fluidized beds based on the height to bed diameter ratio. *Powder Technol.* **2012**, *228*, 264–271. [\[CrossRef\]](#)
68. Shaul, S.; Rabinovich, E.; Kalman, H. Typical fluidization characteristics for Geldart's classification groups. *Part. Sci. Technol.* **2014**, *32*, 197–205. [\[CrossRef\]](#)
69. Kong, W.; Tan, T.; Baeyens, J.; Flamant, G.; Zhang, H. Bubbling and Slugging of Geldart Group A Powders in Small Diameter Columns. *Ind. Eng. Chem. Res.* **2017**, *56*, 4136–4144. [\[CrossRef\]](#)
70. Abrahamsen, A.R.; Geldart, D. Behaviour of gas-fluidized beds of fine powders part I. Homogeneous expansion. *Powder Technol.* **1980**, *26*, 35–46. [\[CrossRef\]](#)
71. Rowe, P.N.; Yacono, C.X.R. The bubbling behaviour of fine powders when fluidised. *Chem. Eng. Sci.* **1976**, *31*, 1179–1192. [\[CrossRef\]](#)
72. Rowe, P.N.; Partridge, B.A. X-ray study of bubbles in fluidized beds. *Process Saf. Environ. Prot. Trans. Inst. Chem. Eng. Part B* **1965**, *43*, 157–175.
73. Rowe, P.N.; Partridge, B.A. An X-ray study of bubbles in fluidised beds. *Chem. Eng. Res. Des.* **1997**, *75*, S116–S134. [\[CrossRef\]](#)
74. Rowe, P.N.; Everett, D.J. Fluidised bed bubbles viewed by X-rays. Part I: Experimental details and the interaction of bubbles with solid surfaces. *Trans. Inst. Chem. Eng.* **1972**, *50*, 42–48.
75. Yacono, C.X.R. An X-Ray Study of Bubbles in Gas-Fluidised Beds of Small Particles. Ph.D. Thesis, University College London, London, UK, 1975.
76. Rowe, P.N. A note on the motion of a bubble rising through a fluidized bed. *Chem. Eng. Sci.* **1964**, *19*, 75–77. [\[CrossRef\]](#)
77. Rowe, P.N. Prediction of bubble size in a gas fluidised bed. *Chem. Eng. Sci.* **1976**, *31*, 285–288. [\[CrossRef\]](#)
78. Yang, W. *Handbook of Fluidization and Fluid-Particle Systems*; CRC Press: New York, NY, USA, 2003.
79. Whitehead, A.B.; Gartside, G.; Dent, D.C. Fluidization studies in large gas-solid systems. Part III. The effect of bed depth and fluidizing velocity on solids circulation patterns. *Powder Technol.* **1976**, *14*, 61–70. [\[CrossRef\]](#)

80. Geldart, D. The size and frequency of bubbles in two- and three-dimensional gas-fluidised beds. *Powder Technol.* **1970**, *4*, 41–55. [[CrossRef](#)]
81. Werther, J. Bubble growth in large diameter fluidized beds. *Fluid Technol.* **1975**, *1*, 215.
82. Mori, S.; Wen, C.Y. Estimation of bubble diameter in gaseous fluidized beds. *AIChE J.* **1975**, *21*, 109–115. [[CrossRef](#)]
83. Cai, P.; Schiavetti, M.; de Michele, G.; Grazzini, G.C.; Miccio, M. Quantitative estimation of bubble size in PFBC. *Powder Technol.* **1994**, *80*, 99–109. [[CrossRef](#)]
84. Darton, R.C.; Nauze, R.; Harrison, D.; Davidson, J. Bubble Growth due to Coalescence in Fluidised Beds. In *Chemical Reactor Theory*; Lapidus, I., Amundson, N.R., Eds.; Prentice-Hall: New York, NY, USA, 1977.
85. Horio, M.; Nonaka, A. A generalized bubble diameter correlation for gas-solid fluidized beds. *AIChE J.* **1987**, *33*, 1865–1872. [[CrossRef](#)]
86. Rowe, P.N. *Experimental Properties of Bubbles. Fluidization*; Academic Press: New York, NY, USA, 1971; p. 121.
87. Harrison, D.; Davidson, J.F.; de Kock, J.W. Bubble growth theory in fluidized beds. *Chem. Eng. Sci.* **1961**, *39*, 202.
88. Davidson, J.F.; Harrison, D. *Fluidized Particles*; Cambridge University Press: Cambridge, NY, USA, 1963.
89. Upson, P.C.; Pyle, D.L. The Stability of Bubbles in Fluidized Beds. In *Fluidization and its Applications: Proceedings of the International Symposium*; Cepadues Edition: Toulouse, France, 1973; pp. 207–222.
90. Clift, R.; Grace, J.R.; Weber, M.E. Stability of Bubbles in Fluidized Beds. *Ind. Eng. Chem. Fundam.* **1974**, *13*, 45–51. [[CrossRef](#)]
91. Rice, W.J.; Wilhelm, R.H. Surface dynamics of fluidized beds and quality of fluidization. *AIChE J.* **1958**, *4*, 423–429. [[CrossRef](#)]
92. Karimipour, S.; Pugsley, T. A critical evaluation of literature correlations for predicting bubble size and velocity in gas–solid fluidized beds. *Powder Technol.* **2011**, *205*, 1–14. [[CrossRef](#)]
93. Davies, R.M.; Taylor, G.I. The mechanics of large bubbles rising through extended liquids and through liquids in tubes. *Proc. R. Soc. Lond. Ser. A Math. Phys. Sci.* **1950**, *200*, 375–390. [[CrossRef](#)]
94. Sit, S.P.; Grace, J.R. Effect of bubble interaction on interphase mass transfer in gas fluidized beds. *Chem. Eng. Sci.* **1981**, *36*, 327–335. [[CrossRef](#)]
95. Chiba, T.; Kobayashi, H. Solid exchange between the bubble wake and the emulsion phase in a gas-fluidised bed. *J. Chem. Eng. Jpn.* **1977**, *10*, 206–210. [[CrossRef](#)]
96. Pyle, D.L.; Harrison, D. An experimental investigation of the two-phase theory of fluidization. *Chem. Eng. Sci.* **1967**, *22*, 1199–1207. [[CrossRef](#)]
97. Pyle, D.L.; Harrison, D. The rising velocity of bubbles in two-dimensional fluidised beds. *Chem. Eng. Sci.* **1967**, *22*, 531–535. [[CrossRef](#)]
98. Marsheck, R.M.; Gomezplata, A. Particle flow patterns in a fluidized bed. *AIChE J.* **1965**, *11*, 167–173. [[CrossRef](#)]
99. Gabor, J.D. On the mechanics of fluidized particle movement. *Chem. Eng. J.* **1972**, *4*, 118–126. [[CrossRef](#)]
100. Stein, M.; Ding, Y.L.; Seville, J.P.K.; Parker, D.J. Solids motion in bubbling gas fluidized beds. *Chem. Eng. Sci.* **2000**, *55*, 5291–5300. [[CrossRef](#)]
101. Mostoufi, N.; Chaouki, J. Local solid mixing in gas–solid fluidized beds. *Powder Technol.* **2001**, *114*, 23–31. [[CrossRef](#)]
102. Shabaniyan, J.; Chaouki, J. Influence of interparticle forces on solids motion in a bubbling gas-solid fluidized bed. *Powder Technol.* **2016**, *299*, 98–106. [[CrossRef](#)]
103. Werther, J.; Molerus, O. The local structure of gas fluidized beds -II. The spatial distribution of bubbles. *Int. J. Multiph. Flow* **1973**, *1*, 123–138. [[CrossRef](#)]
104. Callcott, T.G.; Rigby, G.R.; Singh, B. Experiences in the handling of particulate materials. *BHP Tech. Bull.* **1975**, *19*, 20.
105. Gabor, J.D. Lateral solids mixing in fluidized-packed beds. *AIChE J.* **1964**, *10*, 345–350. [[CrossRef](#)]
106. Hiram, T.; Ishida, M.; Shirai, T. The Lateral Dispersion of Solid Particles in Fluidized Beds. *Kagaku Kogaku Ronbunshu* **1975**, *1*, 272–276. [[CrossRef](#)]
107. Mori, Y.; Nakamura, K. Solid Mixing in Fluidised Bed. *Chem. Eng.* **1965**, *29*, 868–875. [[CrossRef](#)]
108. Fan, L.T.; Shl, Y.F. Lateral Mixing of Solids in Batch Gas-Solids Fluidized Beds. *Ind. Eng. Chem. Process Des. Dev.* **1984**, *23*, 337–341. [[CrossRef](#)]
109. Merry, J. Gulf stream circulation in shallow fluidized beds. *Trans. Inst. Chem. Eng.* **1973**, *51*, 361–368.
110. Grace, J.R. Processes. In *AIChE Symposium Series*; McGill Univ.: Montreal, QC, Canada, 1974.
111. Harris, B.J. Modeling options for circulating fluidized beds: A core/annulus deposition model. *Circ. Fluid. Bed Technol.* **1994**, 32–39.
112. Grace, J.R.; Clift, R. On the two-phase theory of fluidization. *Chem. Eng. Sci.* **1974**, *29*, 327–334. [[CrossRef](#)]
113. Rowe, P.N. A model for chemical reaction in the entry region of a gas fluidised-bed reactor. *Chem. Eng. Sci.* **1993**, *48*, 2519–2524. [[CrossRef](#)]
114. Sane, S.U.; Haynes, H.W.; Agarwal, P.K. An experimental and modelling investigation of gas mixing in bubbling fluidized beds. *Chem. Eng. Sci.* **1996**, *51*, 1133–1147. [[CrossRef](#)]
115. Rowe, P.N. *Two-Phase Theory and Fluidized Bed Reactor Models*; ACS Symposium Series; ACS: Houston, TX, USA, 1978; Volume 65, pp. 436–446. [[CrossRef](#)]
116. Darton, R. A Bubble growth theory of fluidised bed reactors. *Trans. Inst. Chem. Eng.* **1979**, *57*, 134–138.
117. Behie, L.A.; Kehoe, P. The grid region in a fluidized bed reactor. *AIChE J.* **1973**, *19*, 1070–1072. [[CrossRef](#)]

118. Markhevka, V.I.; Basov, V.A.; Melik-Akhazarov, T.K.; Orochko, D.I. The flow of a gas jet into a fluidized bed. *Theor. Found. Chem. Eng.* **1971**, *5*, 80.
119. Kececioglu, I.; Yang, W.-C.; Keairns, D.L. Fate of solids fed pneumatically through a jet into a fluidized bed. *AIChE J.* **1984**, *30*, 99–110. [[CrossRef](#)]
120. Rowe, P.N.; MacGillivray, H.J.; Cheesman, D. Gas discharge from an orifice into a gas fluidised bed. *Trans. Inst. Chem. Eng.* **1979**, *57*, 194–199.
121. Kozin, V.E.; Baskakov, A.P. A study of the grating region of fluidized bed above bubble-cap-type gas-distributors. *Chem. Technol. Fuels Oils* **1967**, *3*, 544–547. [[CrossRef](#)]
122. Baerns, M.; Fetting, F. Quenching of a Hot Gas Stream in a Gas Fluidized Bed. *Chem. Eng. Sci.* **1964**, *20*, 273–280. [[CrossRef](#)]
123. Merry, J.M.D. Fluid and particle entrainment into vertical jets in fluidized beds. *AIChE J.* **1976**, *22*, 315–323. [[CrossRef](#)]
124. Merry, J.M.D. Penetration of vertical jets into fluidized beds. *AIChE J.* **1975**, *21*, 507–510. [[CrossRef](#)]
125. Kunii, D.; Levenspiel, O.; Levenspiel, O. Fluidized Reactor Models. 1. For Bubbling Beds of Fine, Intermediate, and Large Particles. 2. For the Lean Phase: Freeboard and Fast Fluidization. *Ind. Eng. Chem. Res.* **1990**, *29*, 1226–1234. [[CrossRef](#)]
126. Levenspiel, O.; Kunii, D.; Fitzgerald, T. The processing of solids of changing size in bubbling fluidized beds. *Powder Technol.* **1968**, *2*, 87–96. [[CrossRef](#)]
127. Cooke, M.J.; Harris, W.; Highley, J.; Williams, D.F. Kinetics of oxygen consumption in fluidized bed carbonizers. *Tripart. Chem. Eng. Conf. Symp. Fluid. I* **1968**, *30*, 14–20.
128. Kumar, S.; Chadha, A.; Gupta, R.; Sharma, R. CATCRACK: A Process Simulator for an Integrated FCC-Regenerator System. *Ind. Eng. Chem. Res.* **1995**, *34*, 3737–3748. [[CrossRef](#)]
129. de Lasa, H.I.; Errazu, A.; Barreiro, E.; Solioz, S. Analysis of fluidized bed catalytic cracking regenerator models in an industrial scale unit. *Can. J. Chem. Eng.* **1981**, *59*, 549–553. [[CrossRef](#)]
130. Errazu, A.F.; de Lasa, H.I.; Sarti, F. Fluidized bed catalytic cracking regenerator model: Grid effects. *Can. J. Chem. Eng.* **1979**, *57*, 2.
131. Filho, R.M.; Batista, L.M.F.L.; Fusco, M. A fast fluidized bed reactor for industrial FCC regenerator. *Chem. Eng. Sci.* **1996**, *51*, 1807–1816. [[CrossRef](#)]
132. Faltsi-Saravelou, O.; Vasalos, I.A.; Dimogiorgas, G. FBSim: A model for fluidized bed simulation-II. Simulation of an industrial fluidized catalytic cracking regenerator. *Comput. Chem. Eng.* **1991**, *15*, 647–656. [[CrossRef](#)]
133. Krishna, A.S.; Parkin, E.S. Modeling the regenerator in commercial fluid catalytic cracking units. *Chem. Eng. Prog.* **1985**, *81*, 55–62.
134. Penteado, J.C.; Rossi, L.F.; Negrão, C.O. Numerical Modelling of a FCC Regenerator. In Proceedings of the 17th International Congress of Mechanical Engineering (COBEM), Sao Paulo, Brazil, 10–14 November 2003.
135. Fernandes, J.L.; Verstraete, J.J.; Pinheiro, C.I.C.; Oliveira, N.M.C.; Ramôa Ribeiro, F. Dynamic modelling of an industrial R2R FCC unit. *Chem. Eng. Sci.* **2007**, *62*, 1184–1198. [[CrossRef](#)]
136. Daly, C.; Tidjani, N.; Martin, G.; Roesler, J. *Détermination des Paramètres Cinétiques dans la Régénération des Catalyseurs de FCC*; Technical Report No. 56010; Institut Français du Pétrole (IFP): Paris, France, 2001.
137. Zwinkels, M. FCC Regenerator Simulation Model. Ph.D. Thesis, Institute Français du Pétrole (IFP), Paris, France, 1997.
138. Shaikh, A.A.; Al-Mutairi, E.M.; Ino, T. Modeling and simulation of a downer-type HS-FCC unit. *Ind. Eng. Chem. Res.* **2008**, *47*, 9018–9024. [[CrossRef](#)]
139. Dasila, P.K.; Choudhury, I.; Saraf, D.; Chopra, S.; Dalai, A. Parametric Sensitivity Studies in a Commercial FCC Unit. *Adv. Chem. Eng. Sci.* **2012**, *2*, 136–149. [[CrossRef](#)]
140. Kim, S.; Urm, J.; Kim, D.S.; Lee, K.; Lee, J.M. Modeling, simulation and structural analysis of a fluid catalytic cracking (FCC) process. *Korean J. Chem. Eng.* **2018**, *35*, 2327–2335. [[CrossRef](#)]
141. Grace, J.R. *Fluidized Bed Reactor Modeling*; ACS Symposium Series; ACS: Washington, DC, USA, 1981; Volume 22, pp. 3–18. [[CrossRef](#)]
142. Levenspiel, O. Difficulties in trying to model and scale-up the Bubbling Fluidized Bed (BFB) reactor. *Ind. Eng. Chem. Res.* **2008**, *47*, 273–277. [[CrossRef](#)]
143. Faltsi-Saravelou, O.; Vasalos, I.A. FBSim: A model for fluidized bed simulation-I. Dynamic modeling of an adiabatic reacting system of small gas fluidized particles. *Comput. Chem. Eng.* **1991**, *15*, 639–646. [[CrossRef](#)]
144. Singh, R.; Gbordzoe, E. Modeling FCC spent catalyst regeneration with computational fluid dynamics. *Powder Technol.* **2017**, *316*, 560–568. [[CrossRef](#)]
145. de Lasa, H.I.; Grace, J.R. The influence of the freeboard region in a fluidized bed catalytic cracking regenerator. *AIChE J.* **1979**, *25*, 984–991. [[CrossRef](#)]
146. Cao, B.; Zhang, P.; Zheng, X.; Xu, C.; Gao, J. Numerical simulation of hydrodynamics and coke combustions in FCC regenerator. *Pet. Sci. Technol.* **2008**, *26*, 256–269. [[CrossRef](#)]
147. Wu, C.; Cheng, Y.; Ding, Y.; Jin, Y. CFD-DEM simulation of gas-solid reacting flows in fluid catalytic cracking (FCC) process. *Chem. Eng. Sci.* **2010**, *65*, 542–549. [[CrossRef](#)]
148. Latham, R.; Potter, O.E. Back-mixing of gas in a 6-in diameter fluidised bed. *Chem. Eng. J.* **1970**, *1*, 152–162. [[CrossRef](#)]
149. Rowe, P.N.; Partridge, B.A.; Cheney, A.G.; Henwood, G.A.; Lyall, E. Mechanisms of solids mixing in fluidised beds. *Trans. Inst. Chem. Eng. Chem. Eng.* **1965**, *43*, T271.
150. Liu, D.; Chen, X. Lateral solids dispersion coefficient in large-scale fluidized beds. *Combust. Flame* **2010**, *157*, 2116–2124. [[CrossRef](#)]

151. Olsson, J.; Pallarès, D.; Johnsson, F. Lateral fuel dispersion in a large-scale bubbling fluidized bed. *Chem. Eng. Sci.* **2012**, *74*, 148–159. [[CrossRef](#)]
152. Fan, L.T.; Song, J.C.; Yutani, N. Radial particle mixing in gas-solids fluidized beds. *Chem. Eng. Sci.* **1986**, *41*, 117–122. [[CrossRef](#)]
153. IPCC. *Climate Change and Land an IPCC Special Report on Climate Change, Desertification, Land Degradation, Sustainable Land Management, Food Security, and Greenhouse Gas Fluxes in Terrestrial Ecosystems*; IPCC: Geneva, Switzerland, 2019.
154. le Quéré, C.; Andrew, R.M.; Friedlingstein, P.; Sitch, S.; Hauck, J.; Pongratz, J.; Pickers, P.A.; Korsbakken, J.; Peters, G.P.; Canadell, J.G.; et al. Global Carbon Budget 2018. *Earth Syst. Sci. Data* **2018**, *10*, 2141–2194. [[CrossRef](#)]
155. Scala, F. *Fluidized Bed Technologies for Near-Zero Emission Combustion and Gasification*; Woodhead Publishing Limited: Cambridge, UK, 2013.
156. Nakhaei, M.; Lu, B.; Tian, Y.; Wang, W.; Dam-Johansen, K.; Wu, H. CFD Modeling of Gas–Solid Cyclone Separators at Ambient and Elevated Temperatures. *Processes* **2020**, *8*, 228. [[CrossRef](#)]
157. Wang, B.; Xu, D.L.; Chu, K.W.; Yu, A.B. Numerical study of gas–solid flow in a cyclone separator. *Appl. Math. Model.* **2006**, *30*, 1326–1342. [[CrossRef](#)]
158. Hashemi Shahraki, B. The Development and Validation of New Equations for Prediction of the Performance of Tangential Cyclones. *Int. J. Eng.* **2003**, *16*, 109–124.
159. Lu, C.-X. FCC riser quick separation system: A review. *Pet. Sci.* **2016**, *13*, 776–781. [[CrossRef](#)]
160. Wei, Q.; Sun, G.; Yang, J. A model for prediction of maximum-efficiency inlet velocity in a gas-solid cyclone separator. *Chem. Eng. Sci.* **2019**, *204*, 287–297. [[CrossRef](#)]
161. Chu, K.W.; Wang, B.; Xu, D.L.; Chen, Y.X.; Yu, A.B. CFD–DEM simulation of the gas–solid flow in a cyclone separator. *Chem. Eng. Sci.* **2011**, *66*, 834–847. [[CrossRef](#)]
162. Masnadi, M.S.; Grace, J.R.; Elyasi, S.; Bi, X. Distribution of multi-phase gas–solid flow across identical parallel cyclones: Modeling and experimental study. *Sep. Purif. Technol.* **2010**, *72*, 48–55. [[CrossRef](#)]
163. Zhang, R.; Basu, P. A simple model for prediction of solid collection efficiency of a gas–solid separator. *Powder Technol.* **2004**, *147*, 86–93. [[CrossRef](#)]
164. Jiang, Y.; Qiu, G.; Wang, H. Modelling and experimental investigation of the full-loop gas–solid flow in a circulating fluidized bed with six cyclone separators. *Chem. Eng. Sci.* **2014**, *109*, 85–97. [[CrossRef](#)]
165. Baltrnas, P.; Vaitiekūnas, P.; Jakštonienn, I.; Konoverskytt, S. Study of gas-solid flow in a multichannel cyclone. *J. Environ. Eng. Landsc. Manag.* **2012**, *20*, 129–137. [[CrossRef](#)]
166. Su, Y.; Mao, Y. Experimental study on the gas–solid suspension flow in a square cyclone separator. *Chem. Eng. J.* **2006**, *121*, 51–58. [[CrossRef](#)]
167. Lapple, C.E. Gravity and Centrifugal Separation. *Am. Ind. Hyg. Assoc. Q.* **1950**, *11*, 40–48. [[CrossRef](#)]
168. Gimbin, J.; Chuah, T.G.; Choong, T.S.Y.; Fakhru’l-Razi, A. A CFD Study on the Prediction of Cyclone Collection Efficiency. *Int. J. Comput. Methods Eng. Sci. Mech.* **2006**, *6*, 161–168. [[CrossRef](#)]
169. Dirgo, J.; Leith, D. Aerosol Science and Technology Cyclone Collection Efficiency: Comparison of Experimental Results with Theoretical Predictions. *Exp. Results Theor. Predict. Aerosol Sci. Technol.* **2007**, *4*, 401–415. [[CrossRef](#)]
170. Cortés, C.; Gil, A. Modeling the gas and particle flow inside cyclone separators. *Prog. Energy Combust. Sci.* **2007**, *33*, 409–452. [[CrossRef](#)]
171. Morin, M.; Raynal, L.; Karri, S.B.R.; Cocco, R. Effect of solid loading and inlet aspect ratio on cyclone efficiency and pressure drop: Experimental study and CFD simulations. *Powder Technol.* **2021**, *377*, 174–185. [[CrossRef](#)]
172. Rosin, P.; Rammmler, E.; Intelmann, W. Principles and limits of cyclone dust removal. *Zeit Ver Dtsch. Ing.* **1932**, *76*, 433–437.
173. Maheshwari, F.; Parmar, A. A Review Study on Gas-Solid Cyclone Separator using Lapple Model. *J. Res.* **2018**, *4*, 1–5.
174. Hoffmann, A.C.; Stein, L.E. *Computational Fluid Dynamics. Gas Cyclones and Swirl Tubes*, Berlin, Heidelberg; Springer: Berlin/Heidelberg, Germany, 2002; pp. 123–135. [[CrossRef](#)]
175. Chen, J.; Shi, M. A universal model to calculate cyclone pressure drop. *Powder Technol.* **2007**, *171*, 184–191. [[CrossRef](#)]
176. Knowlton, T.; Karri, R.S.B. Differences in cyclone operation at low and high solids loading. In Proceedings of the International Fluidization South Africa Conference, Johannesburg, South Africa, 19–20 November 2008; pp. 119–160.
177. Li, S.; Yang, H.; Wu, Y.; Zhang, H. Improved cyclone pressure drop model at high inlet solid concentrations. *Chem. Eng. Technol.* **2011**, *34*, 1507–1513. [[CrossRef](#)]
178. Casal, J.; Martinez-Benet, J.M. A better way to calculate cyclone pressure drop. *Chem. Eng.* **1983**, *90*, 99–100.